Conjugative transfer inhibition of IncA and IncC plasmids by pervasive SGI1-like elements via relaxosome assembly interference

Florence Deschênes,[a] Romain Durand,[a*1], Kevin T. Huguet,[a*2], Nicolas Rivard,[a*3], Chloé Chagnon,[a] Doriane Planez,[a] & Vincent Burrus,[a#]

[a]Département de biologie, Université de Sherbrooke, Sherbrooke, J1K 2R1, Québec, Canada

Running Head: Fertility inhibition of IncA and IncC plasmid by SGI1

#Address correspondence to Vincent Burrus, vincent.burrus@usherbrooke.ca. Tel: 819 821-8000 #65223; Fax: 819 821-8049

*[1]Present address: Institut de Biologie Intégrative et des Systèmes, Université Laval, Québec, Canada

*[2]Present address: CNRS, LCPME, UMR 7564, Université de Lorraine, Villers-lès-Nancy, France

*[3]Present address: Laboratoire d'Ingénierie des Systèmes Macromoléculaires, UMR7255, Institut de Microbiologie de la Méditerranée, Aix Marseille Université, CNRS, Marseille, France

Abstract word count: 250 words

Text word cound: 5570

ABSTRACT

Broad-host-range IncA and IncC conjugative plasmids propagate multidrug resistance in bacteria and mobilize chromosomal resistance islands, including *Salmonella* Genomic Island 1 (SGI1) across genera. Mobilization of SGI1 and kin usually occurs at rates orders of magnitude higher than plasmid transfer, which seems inhibited. Here, we identified, using a Tnseq approach, a broadly conserved fertility inhibitor, which we name CtiC (for 'Conjugative Transfer Inhibition of IncC'), encoded by SGI1 and kin that hampers helper plasmid transfer. *ctiC* expression is constitutive and elicited by the transcriptional activator of the transfer genes of IncA and IncC plasmids. *ctiC* suppression greatly enhances IncC plasmid transfer, indicating it counters a general improvement of conjugation mediated by SGI1. Our results show that the two genes *traHG* located upstream of *ctiC* in SGI1 account for the enhanced transfer properties. CtiC specifically prevents the cotransfer of the helper plasmid, which impairs SGI1 stability in transconjugants. A comparison of structural predictions revealed that the inhibitor resembles the C-terminus of the MOB_{H12}-family relaxase TraI of IncA and IncC plasmids despite low sequence conservation. Distant CtiC homologues sharing the same predicted structure exhibit similar inhibitory activities. Bacterial two-hybrid assays and relaxase domain substitution show that CtiC interferes with relaxosome assembly that initiates plasmid transfer. We show that CtiC binds to the mobilization factor MobI of IncC plasmids, a key protein that recognizes the origin of transfer, thus preventing its interaction with TraI. Our work reveals a fertility inhibition mechanism that prevents relaxosome assembly and uncovers a functional domain in MOB_{H12} relaxases.

IMPORTANCE

IncA and IncC conjugative plasmids and mobile genetic elements they mobilize, such as the *Salmonella* Genomic Island 1 (SGI1), drive the dissemination of multidrug resistance across Enterobacteriaceae and Vibrionoceae. Surprisingly, SGI1 and related elements inhibit the

transfer of their helper plasmids. Here, we identified the SGI1-encoded factor that impairs helper plasmid transfer. We showed it interferes with the assembly of the relaxosome, a protein complex recruited at the *cis*-acting origin of transfer (*oriT*), where the TraI initiates DNA transfer upon binding to the mobilization factor, MobI. Structural resemblances between the fertility inhibition factor and TraI C-terminus reveal the mechanism of transfer inhibition and the binding site of MobI to MOB_{H12} relaxases, which are poorly characterized and could be a target to curb resistance gene propagation. Given the prevalence of SGI1-like elements in bacterial genomes, this work also provides insights into their influence on IncA and IncC plasmid dissemination in bacterial pathogens.

INTRODUCTION

Bacterial genomes can host a rich and diverse bestiary of mobile genetic elements (MGEs). Self-transmissible MGEs, such as conjugative plasmids and integrative and conjugative elements (ICEs), facilitate the exchange of antibiotic-resistance genes (ARGs) between bacteria by spreading from host to host via conjugation, a mechanism relying on a type IV secretion system (T4SS) that injects their DNA into recipient cells (1–4). Other MGEs, called integrative and mobilizable elements (IMEs), lack the genes required for self-transmissibility and coopt the T4SS encoded by helper conjugative MGEs to propagate (5, 6).

Conjugative plasmids of the incompatibility group C (IncC) contribute to the pervasive spread of ARGs across taxonomic barriers in pathogenic species of *Enterobacteriaceae*, *Vibrionaceae*, *Yersiniaceae*, and *Morganellaceae* in healthcare settings, animal husbandry and the environment (7). IncC and related IncA plasmids (collectively referred to as A/C plasmids) share a ~128-kb set of core genes (>93% identity) disrupted by insertions of variable DNA and ARGs (8–12). Among the conserved genes are those involved in plasmid replication and partition, conjugative transfer (*tra* genes and operons, and *mobI*), entry and surface exclusion, DNA repair, and regulation (*acaB*, *acaDC*, *acr1*, *acr2*) (8, 13–21). The conjugative transfer of A/C plasmids is initiated at the origin of transfer (*oriT*), a cis-acting locus located upstream of *mobI* (8, 19). The mobilization factor MobI is thought to bind to *oriT* and recruit the MOB_{H12} family relaxase TraI, which initiates the intercellular rolling-circle replication of the DNA to transfer.

Besides self-propagation, A/C plasmids promote the transmission of multiple IMEs, including the ARGs-bearing 43-kb *Salmonella* Genomic Island 1 (SGI1) (22–24). SGI1 and its variants typically integrate at the 3' end of *trmE* in a broad range of bacterial species, including *Proteus mirabilis* (PGI1), *Acinetobacter baumannii* (AGI1), and *Vibrio cholerae* (GI-15) (25). Distant relatives of SGI1 have also been found integrated at alternative sites (*dusA* and *yicC*) (26). One of their representatives, IME*Vch*USA3 of *V. cholerae*, lacks ARGs but remains mobilizable by

A/C plasmids. Despite encoding different integrases targeting different integration sites, all SGI1-related IMEs share a small set of conserved genes that play a crucial role in their mobilization. Among those, *mpsAB* encodes the relaxase that recognizes and processes their *oriT* independently of the relaxase TraI of A/C plasmids (27). Also conserved are *traG* (and often abutting gene *traH*) and *traN*, which encode distant orthologues of the corresponding mating pair formation protein TraG and mating pair stabilization protein TraN of A/C plasmids (13, 26).

Past reports showed that SGI1 or its variants can drastically inhibit (up to 2- to 3-log decrease) the transfer of A/C plasmids and that transconjugants carrying both the IME and its helper plasmid are rare (14, 22, 28–30). Competition for the T4SS is an attractive hypothesis that could explain part of the inhibition of helper plasmid transfer by an IME. However, competition alone is unlikely to result in such a drastic effect unless SGI1-like IMEs encode factors that skew the T4SS to selectively enhance IME mobilization or inhibit helper plasmid transfer, a phenomenon evocative of fertility inhibition observed between unrelated plasmids (31).

Here, we leveraged transposon-directed insertion sequencing (TraDIS) to identify SGI1 genes that negatively affect the transfer of a helper IncC plasmid. We report that a small, conserved gene located immediately downstream of *traG* is solely responsible for inhibiting the transfer of the helper A/C plasmids. Structural modelling and bacterial double-hybrid assays suggest fertility inhibition results from relaxosome assembly interference. Furthermore, our results indicate that fertility inhibition offsets a general improvement of the IncC conjugative apparatus promoted by SGI1, likely to prevent the cotransfer of the IME and its helper plasmid, which otherwise destabilizes the IME in transconjugants.

RESULTS

Identification of SGI1 genes that inhibit IncC plasmid transfer

Since SGI1 strongly inhibits A/C plasmid transfer, we hypothesized that disruption of SGI1 inhibitory genes should restore wild-type transfer of the IncC plasmid pVCR94 and increase the population of transconjugants harbouring both SGI1 and pVCR94. Hence, we performed a transposon-directed insertion sequencing (TraDIS) assay designed to enrich SGI1 mutants allowing the cotransfer and establishment of pVCR94 in recipients (Fig. 1A). We constructed a library of high-density random mini-Tn*5* insertion in *E. coli* KH95 bearing pVCR94^{Km} Δ*acr2* and SGI1^{Cm}. Removal of *acr2*, the primary repressor of A/C plasmid transfer, increases conjugative transfer, preventing an insertion bias in this negative regulator gene. The resulting mutants composed the input library enriched in mini-Tn*5* insertions that enable plasmid replication and coexistence with SGI1. We used the input library in a mating assay to transfer the transmissible set of mini-Tn*5*-bearing plasmids and SGI1^{Cm} to *E. coli* GG56 (Nx^{r}). We then selected transconjugants that had acquired both pVCR94^{Km} and SGI1^{Cm} to make up the output library. High-throughput Illumina sequencing of the input and output libraries mapped the mini-Tn*5* insertion sites. An excess of insertions in the output compared to the input was expected to reveal IncC plasmid or SGI1 genes that inhibit the cotransfer.

Before all else, we could not detect any statistically significant mini-Tn*5* insertion enrichment in the output for pVCR94^{Km}, suggesting that no gene of the helper plasmid harms the mobilization of SGI1 in our conditions. In contrast, the 2.1-kb region of SGI1 bordered by *traN* and *traG* contained the bulk of mini-Tn*5* insertions (Fig. 1B). More specifically, a small open reading frame of unknown function, S010, was the most frequently disrupted gene (Fig. 1B and 1C). For this reason, S010 was renamed *ctiC* for conjugative transfer inhibitor of IncC. To confirm the involvement of *ctiC* in transfer inhibition, we performed a 2-h *E. coli* mating assay using donors bearing pVCR94^{Sp} and SGI1^{Km} or its Δ*ctiC* mutant. Whereas the presence of SGI1^{Km} reduced the transfer of pVCR94^{Sp} by 4.6-fold, deleting *ctiC* increased

pVCR94^{Sp} transfer by ~305-fold and the cotransfer by ~428-fold (Fig. 1D). This deletion reduced the mobilization of SGI1^{Km} by 7.6-fold. Surprisingly, pVCR94^{Sp} transfer was enhanced (66-fold) in the presence of SGI1 Δ*ctiC*, reaching a level comparable to the IME. This observation indicates that SGI1 improves the transfer of IncC plasmids if *ctiC* is missing.

The Δ*ctiC* mutant was complemented only upon ectopic expression of *ctiC* in the donor, not the recipient. The complementation inhibited IncC plasmid transfer and the cotransfer, albeit not as strongly as wild-type SGI1 (Fig. 1D). Altogether, these results indicate that the product of *ctiC* acts by interfering with a conjugative process occurring in donor cells, not during the establishment of the plasmid in the recipient cell. Finally, we observed that SGI1 also inhibits the transfer of the IncA plasmid pRA1 in a *ctiC*-dependant manner (Fig. S1), despite their divergence from IncC plasmids.

CtiC specifically affects the transfer of A/C plasmids

To test whether CtiC affected the T4SS or the processing of A/C plasmid DNA, we first tested the impact of CtiC on the mobilization of pSU4628, an ampicillin-resistant derivative of pCloDF13. This plasmid is mobilizable by a broad range of conjugative plasmids (IncF, I, N, P, W, and C) (13, 32). pCloDF13 encodes two proteins, MobB and MobC, required to process its *oriT* for mobilization (33). MobC is the relaxase (MOB$_C$ family), whereas MobB, necessary for efficient *oriT* cleavage, acts as a type IV coupling protein. We used pVCR94^{Sp} with SGI1^{Km} or its Δ*ctiC* mutant to mobilize pSU4628. Surprisingly, SGI1 increased the IncC-mediated mobilization of pSU4628 by more than 2 logs regardless of *ctiC* (Fig. 2A). Hence, CtiC does not impair the DNA processing functions and T4CP of pCloDF13 or the IncC-encoded T4SS, suggesting it affects A/C plasmids specifically. It also confirms that SGI1 enhances the conjugative transfer considerably, not specifically its own. This phenotype could result from the TraHG subunit substitution operated by SGI1 in the T4SS encoded by A/C plasmids (13).

CtiC counteracts the effect of TraHG substitution, which increases IncC plasmid transfer

TraH is involved in mating pair formation/stabilization, whereas TraG is an inner membrane protein involved in mating pair stabilization and entry exclusion. To test whether TraH and TraG substitution enhanced conjugative transfer, we used mutants of SGI1^{Km} lacking *traHG*, *ctiC*, both, or the region encompassing *traN* to *traH* (mutant Δ*tra*$_S$). The deletion of *traHG* slightly reduced the transfer of pVCR94^{Sp} and pRA1, which remained low due to *ctiC*; however, it reduced the transfer of SGI1^{Km} by 800-fold and nearly abolished pVCR94^{Sp} cotransfer (Fig. 2B and S1). Its impact on SGI1^{Km} was more limited when pRA1 was the helper plasmid, probably due to its higher transfer rate in our experimental conditions.

Nevertheless, the mutant Δ*traHG* Δ*ctiC* failed to enhance the transmissibility of the helper plasmids, though it restored their transfer to wild-type levels (Fig. 2B and S1). All transfer frequencies using SGI1^{Km} Δ*traHG* Δ*ctiC* were indistinguishable from those obtained using SGI1^{Km} Δ*tra*$_S$, which lacks *traN*, *sgaDC*, *ctiC*, two open reading frames of unknown function, and *traHG* (Fig. 1B, 2B and S1). These results indicate that TraH and TraG of SGI1 are necessary to enhance the conjugative properties of the T4SS encoded by IncC plasmids. Furthermore, our observations suggest that *ctiC* specifically targets A/C plasmids to prevent them from benefiting from this enhancement.

CtiC resembles the C-terminal domain of MOB$_{H1}$ relaxases

The translation product of *ctiC* is an 84-amino acid residue, basic protein (pI=10.08) with a predicted winged helix fold resembling the archaeal DNA polymerase holoenzyme subunit PBP2 (PolB1 binding protein 2) (Fig. S2A) (34). The topology of the winged helix fold consists of a bundle of 3 α-helices and two wings of a 3- or 4-strand β-sheet (wing) (35, 36). The surface of CtiC formed by the first half of the helix α1 and β-sheet has a net positive charge, whereas the opposite surface is negatively charged (Fig. S2C). Comparative analysis of CtiC using Blast and HHblits revealed two types of proteins.

First, *ctiC* is conserved in most SGI1-related IMEs integrated at the 3' end of *trmE*, including GI-15 of seventh pandemic *V. cholerae*, PGI2 of *P. mirabilis*, AGI1 of *A. baumannii*, and KGI1 of *K. pneumoniae* (Fig. 3C). A notable exception, SGI1-LK1 of *P. mirabilis*, lacks *ctiC* due to a large deletion (37). IMEs integrated at the 5' end of *dusA* (e.g., CtiC3 of IME*Vch*USA3) or the 3' end of *yicC* (e.g., CtiC2 of IE*Sen*USA1) encode highly divergent CtiC homologues (24 to 33% identity with CtiC of SGI1) (Fig. 3A-C). Like in SGI1, their coding sequence abuts *traG* except for type 3 *dusA*-associated IMEs (e.g., *unk* of IE*Vch*USA5), where it is separated from *traG* by a small ORF of unknown function (Fig. 3A). The evolutionary relationship between the CtiC homologues is congruent with that of their cognate IMEs (26). The CtiC-like proteins encoded by type 3 *dusA*-associated IMEs are the most divergent. Comparison of the predicted 3D structures revealed a similar fold for CtiC, CtiC2 and CtiC3, except for an additional N-terminal α helix (Fig. 3C and S3C). In contrast, Unk of type 3 IMEs folds into a different conformation (Fig. 3B-D and S3C).

Second, CtiC is distantly related to the last 92 amino acid residues of the C-terminal domain (CTD) of the relaxase TraI of A/C plasmids (TraI_C_{92}; 31.2% identity and 51% similarity) (Fig. 3B). A PSI-Blast analysis revealed that the CtiC signature motif exists only in two protein architectures, either as an autonomous entity or associated with a TraI_2 relaxase domain (Fig. S4). CTDs of MOB_{H12} relaxases encoded by distant relatives of A/C plasmids (pAQU1, pAsa4 and pAhD4-1), IncT (Rts1) and IncP-7 (pCAR1) plasmids, and SXT/R391 elements adopt a similar conformation (Fig. S3A and S3C). CTDs of MOB_{H11} relaxases from IncHI1 (R27) and IncHI2 (R478) plasmids are more dissimilar (Fig. S3B and S3C). CTDs of relaxases encoded by A/C and related plasmids form a clade that is distinct from CtiC homologues encoded by SGI1-related IMEs, regardless of their integration site (Fig. 3C). However, the origin of CtiC homologues cannot be clearly ascribed to a single common ancestor (Fig. S4). Correspondence analysis of all predicted structures confirmed that,

except Unk from type 3 IMEs and MOB_{H11} relaxase CTDs, CtiC homologues and MOB_{H12} relaxase CTDs have almost identical conformations (Fig. 3D, S2B, S5A and S5B). Finally, the CTD of the MOB_{H2} relaxase TraI of ICE*clc* (TraI_2_C domain; Pfam PF07515) is unrelated and adopts a different conformation (Fig. 3D, S5A and S5B).

Distantly related CtiC homologues inhibit IncC plasmid transfer

Given the divergence of SGI1-related IMEs inserted at *dusA*, we wondered whether the CtiC homologues they encode could inhibit IncC plasmid transfer. First, we tested the effect of IME*Vch*USA3^{Km} or its Δ*ctiC3* mutant on pVCR94^{Sp} transfer. Deleting *ctiC3* slightly increased (>6-fold) plasmid transfer but had no significant impact on IME mobilization (Fig. 3E). Overexpressing *ctiC3* in donors reduced plasmid transfer by >6-fold and increased IME mobilization by ~30-fold.

Next, we compared the inhibitory activity of *ctiC* of SGI1, IE*Vch*USA2, IME*Vch*USA3, and the distant homologue *unk* of IE*Vch*USA5 in donors bearing pVCR94^{Sp}. *ctiC* genes reduced pVCR94^{Sp} transfer of pVCR94^{Sp} by 38- to 126-fold (Fig. 3F). In contrast, *unk* had no impact. Hence, all but the most distant CtiC homologues inhibit IncC plasmid transfer.

CtiC reveals a MobI-binding domain (MIBD) conserved in MOB_{H12} relaxases

Based on the predicted structural similarity between CtiC and TraI_C_{92}, we hypothesized that TraI's CTD binds to the mobilization factor MobI and that CtiC interacts with MobI, precluding the recruitment of TraI to *oriT*. Thus, we examined possible interactions between CtiC, MobI, and TraI using a bacterial adenylate cyclase-based two-hybrid (BACTH) assay. The T18 or T25 fragments of the split-adenylate cyclase were fused to the N-terminus of each protein. Because cloning of full-length *traI* proved unsuccessful due to possible toxicity, we used TraIΔHD, which lacks the N-terminal TraI_2 HD hydrolase domain (pfam PF07514), for all fusions. The leucine zipper motif of the yeast transcriptional activator GCN4 (Zip) was the positive control. We detected the self-association of MobI, suggesting it works as a dimer or

multimer, but failed to observe CtiC or TraIΔHD self-association (Fig. 4). Likewise, CtiC and TraIΔHD did not interact. In contrast, we detected a high β-galactosidase activity for MobI/CtiC and a low activity for MobI/TraIΔHD, suggesting that MobI directly interacts with CtiC and TraI. These results support TraI's CTD as a MobI-binding domain (hereafter named MIBD) and strongly suggest that CtiC competes with TraI's MIBD to bind to MobI.

Next, we used BACTH assays to test whether MIBD is necessary and sufficient to promote the interaction between TraI and MobI using TraIΔHD mutants lacking segments of unknown function. Domains Dis1 and Dis2 are predicted disordered, whereas domain X is predicted globular with no known structural homologue except in related relaxases (Fig. 5A). We found that despite the absence of Dis1, Dis2, X or combinations of these three domains, MIBD was required and sufficient for binding to MobI (Fig. 5B).

The substitution of MIBD with CtiC allows inefficient conjugative transfer

To confirm that MIBD binds to MobI, we constructed a mutant of pVCR94^{Cm} expressing a chimerical *traI* gene where *ctiC* replaced the coding sequence of MIBD. While the mutation *traI*ΔMIBD::*aph* abolished the transfer of pVCR94^{Cm}, the substitution *traI*ΔMIBD::*ctiC* partially restored its transfer (Fig. 3G). In this case, transfer was detectable after 2 hours at a level ~2,500 times lower than for wild-type *traI* and increased slightly after 6 hours (Fig. S6). This result confirms the crucial role of MIBD in conjugative transfer initiation and that MIBD and CtiC bind to the same partner, MobI. Hence, CtiC inhibits A/C plasmid transfer by competing with MIBD of TraI to recruit MobI.

Relative expression of TraI, MobI, and CtiC supports a competition model of fertility inhibition

ctiC lies immediately downstream of *traG*, suggesting it is the last gene of the *traHG* operon controlled by an AcaCD-responsive promoter (14, 38). To test this, we translationally fused a promoterless *lacZ* reporter gene to the fifth codon of *ctiC* in SGI1^{Km} and *ctiC3* in IME*Vch*USA3 (Fig. 6A). β-galactosidase assays showed that the transcriptional activator

complex AcaCD ectopically expressed from the arabinose-inducible promoter P_{BAD} increased the expression level of the *ctiC*'-'*lacZ* fusions by ~7- and ~4-fold for SGI1 and IME*Vch*USA3, respectively (Fig. 6B). Furthermore, we detected a constitutive expression of *ctiC*, at a level ~4.5 times lower than that of *ctiC3* in non-inducing conditions. Next, we carried out a reverse transcription experiment using a primer located at the 3' end of *ctiC* (ctiC_RT) and RNA obtained from *E. coli* VB112 cells containing SGI1^{Km} with or without pBAD-*acaCD* (Fig. 6A). PCR amplification using the generated cDNA as the template revealed weakly the junction between *traG* and *ctiC* (*traG-ctiC*) in the absence of *acaCD* but not a fragment located within *traH* (Fig. 6C). This observation confirms that *ctiC* is expressed constitutively from a weak promoter within *traG*. Furthermore, we observed a strong signal for both fragments upon expression of *acaCD*, which is consistent with *ctiC* being part of the *traHG* operon driven from the AcaCD-responsive promoter P_{traH}.

We also translationally fused *lacZ* to the fifth codon of *traI* and *mobI* in pVCR94 (Fig. 6A) to quantify the expression of these two genes. *traI* expression was hardly detectable in the absence of *acaCD* and induced ~300-fold in its presence (Fig. 6B). Expression levels of *traI*, *ctiC*, and *ctiC3* were comparable (40, 33, and 76 Miller units, respectively) in inducing conditions. In non-inducing conditions, *ctiC* and *ctiC3* surpassed *traI* expression by 34 and 160 fold, respectively. Finally, *mobI* expression was constitutive and topped the expression of all the other genes by 10- to 6,000-fold (Fig. 6B). Given the apparent strong binding affinity of CtiC for MobI (Fig.4) and assuming all components have similar stabilities, these findings support a model of fertility inhibition where CtiC sequesters MobI, thereby preventing the interactions between TraI and MobI.

DISCUSSION

Fertility inhibition is a process by which a plasmid impairs the conjugation of another coresident plasmid in the donor cells (31). Various fertility inhibition systems target different steps of the conjugation process of coresident plasmids belonging to diverse incompatibility groups. For instance, FinO of IncFII plasmids inhibits the conjugation of the F plasmid by repressing the expression of its transfer genes via an increase of the antisense RNA FinP levels (39). Likewise, FinQ and FinU encoded by IncI1 plasmids and FinW of IncFI plasmids downregulate the expression of transfer genes of F via alternative pathways (40). FinV of IncX plasmids seems to affect the pilus assembly of IncF plasmids (41, 42). Other fertility inhibition systems affect the type IV coupling protein that connects the relaxosome to the T4SS, such as PifC of F that targets TraG of the IncP plasmids or FinC of the mobilizable plasmid CloDF13 that seems to target TraD of F (43, 44). Osa is an oncogenic suppressor encoded by the IncW plasmid pSa that targets the Ti plasmid of *Agrobacterium tumefaciens*. Osa degrades the Ti plasmid-encoded T-DNA attached to the VirD2 relaxase before it is translocated through the T4SS via the coupling protein VirD4 (45). Osa and related factors of the ParB/Srx superfamily have both ATPase and DNase activity.

Here, we found that SGI1 and its distant relative IME*Vch*USA3 inhibit the conjugation of A/C plasmids. The fertility inhibition factor is *ctiC*, a small gene located downstream of *traG* and conserved in several families of SGI1-like IMEs integrated at three different chromosomal loci in their host. CtiC is distantly related to and has a predicted 3D structure resembling the CTD of the $MOBH_{12}$ relaxase TraI encoded by A/C and related untyped conjugative plasmids (Fig. S3). We also provide evidence that CtiC mimics the CTD of TraI, thereby interfering with relaxosome assembly via competition for the essential mobilization factor MobI (Fig. 7), which is necessary for *oriT* recognition (8, 19, 46). To the best of our knowledge, CtiC is the only known fertility inhibition factor interfering with relaxosome assembly.

Except for the relaxases TcpM of pCW3 and MspA of SGI1, which are related to site-specific tyrosine recombinases (DNA_BRE_C superfamily) (27, 47), known relaxases were phylogenetically classified into seven major families (48, 49). MOB_F, MOB_P, MOB_Q, and MOB_V relaxases contain HUH signature motifs of site-specific ssDNA endonucleases (48). MOB_C relaxases resemble restriction endonucleases. MOB_T relaxases are related to rolling-circle replication Rep-Trans proteins (50). Finally, MOB_H relaxases harbour an N-terminal relaxase domain (TraI_2) containing an N-terminal 3H motif reminiscent of the HUH motif and an HD hydrolase motif. The MOB_H family is subdivided into two major clades. (48). The MOB_{H2} clade contains relaxases encoded by ICE*clc* of *Pseudomonas putida* and the Gonococcal Genomic Island (GGI) of *Neisseria gonorrhoeae* (48). These relaxases contain a TraI_2_C CTD of unknown function that forms a globular structure (51). The MOB_{H1} clade is subdivided into two sub-clades. MOB_{H11} includes relaxases encoded by IncHI1 and IncHI2 plasmids. MOB_{H12} contains the relaxases of A/C, IncT, and IncP-7 plasmids and SXT/R391 elements (48). Before this work, no conserved functional domain, except TraI_2, was identified in MOB_{H1} relaxases. We found that the CTD of TraI structurally resembles CtiC and binds the ancillary mobilization factor MobI thought to recognize and bind *oriT* (8, 19). The CTDs of MOB_{H12} and MOB_{H2} relaxases are strikingly different (Fig. S5), and MOB_{H2} relaxases do not seem to require a MobI homolog to initiate DNA transfer. The CTDs of $MOBH_{12}$ and $MOBH_{11}$ relaxases are also dissimilar, but both require a MobI-like mobilization factor (e.g., TraH of R27) (52).

Genes coding for distant homologues of MobI have been found in IMEs unrelated to SGI1, lacking a relaxase gene but mobilized by IncC plasmids in a TraI-dependant fashion (23). In all these instances, an *oriT* unrelated to that of IncC plasmids lies upstream of *mobI* (53). Hence, MobI proteins presumably play an integral part in the specific recognition of *oriT*s by TraI. We showed that MobI interacts with itself to form a multimeric complex (Fig. 4). Based

on this observation, we constructed using Alphafold a dimeric MobI complex, a likely conformation for a DNA-binding protein, that we associated with two subunits of TraI (MIBD domain), two subunits of CtiC, or a combination of both (Fig. 8). We predict that, like the $MobI_2$-$CtiC_2$ complex, the TraI-$MobI_2$-CtiC complex would be ineffective if, like for the F plasmid (MOB_F family of relaxases), two subunits of TraI are required for DNA processing. Further biochemical characterization is necessary to confirm this model.

We found that *ctiC* of SGI1 is part of the *traHG* operon driven by the P_{traH} promoter, which is part of the AcaCD regulon, confirming previous reports (14, 30). This regulation is conserved in IME*Vch*USA3 and presumably all distantly related IMEs. Hence, *ctiC* genes are expressed in conditions that trigger the expression of the transfer genes of A/C plasmids, to which belongs the relaxase gene *traI* (14). P_{traH} also reacts to SgaCD, the SGI1-encoded homologues of AcaCD, whose expression is activated by the SOS response (38, 54). Activation of *ctiC* expression by SgaCD could explain the slight enrichment of mini-Tn*5* insertions in *sgaDC* in our TraDIS experiment (Fig. 1B). The expression levels of *ctiC* and *traI* are strikingly similar in inducing conditions, but *ctiC* and *ctiC3* are constitutively expressed at low level, even in the absence of a helper plasmid (Fig. 6B). This observation suggests that SGI1-like IMEs might prime the cells to quench the conjugative transfer of their helper plasmid as soon as it enters the cell.

The importance of the region encompassing *traN* to *traHG* in the lifecycle of SGI1-like IMEs has long remained controversial (13, 29). Others pointed out that SGI1 variants lacking this 9.7-kb region, such as SGI1-KL1, remain mobilizable despite the absence of three T4SS subunit-encoding genes, the gene *S010*, now known as *ctiC*, and the SOS-response controlled transcriptional activator genes *sgaDC* (37, 55). Though this observation is accurate in laboratory conditions, it underestimates its impact on the evolutionary success of SGI1-related IMEs in a natural context. Indeed, our results using the tra_S and *traHG* mutants

of SGI1 undeniably confirm that the loss of this region drastically impairs SGI1 mobilization (Fig. 2B). *traHG* replacement accounts for the enhanced conjugation phenotype, although the precise mechanism remains elusive. *ctiC* prevents the helper plasmid from benefiting from the improved conjugation efficiency resulting from the TraHG substitution (Fig. 2B). By reducing the odds of cotransfer, CtiC allows the IME to stabilize in its new host. As long as the helper plasmid coresides in the cell, the activator AcaCD elicits the expression of the excisionase of the IME, which remains excised, hence subjected to loss despite its ability to replicate (56, 57). TraH, TraG, and CtiC are, like SgaCD (38), essential components of the SGI1 lifecycle. The weaker impact of *ctiC3* deletion in IME*Vch*USA3 on the helper plasmid compared to *ctiC* deletion in SGI1 (compare Figs 1D and 3E) likely stems from the absence of *traH* and *sgaD* in IME*Vch*USA3 (26).

ctiC is broadly conserved in SGI1-like IMEs dwelling in several pathogenic species of *Enterobacteriaceae* and marine bacteria (*Vibrio*, *Shewanella*) (25, 26). For instance, *ctiC* exists in the IME GI-15 (Fig. S7), which propagated ARGs in clinical isolates of *V. cholerae* O1 El Tor during the second epidemic wave of the 7th cholera pandemic (58, 59). The presence of GI-15 and IncC plasmids in pandemic strains seems inversely correlated (59).

Fertility inhibition is another parasitic behaviours exhibited by SGI1-like IMEs towards A/C plasmids. SGI1 TraG-mediated reshaping of the T4SS has previously been shown to allow SGI1 to dodge IncC (and IncA) entry exclusion mediated by *eexC* (13, 20). Entry exclusion prevents the redundant transfer of a conjugative element into a recipient cell containing the same or a similar element. Entry exclusion avoidance presumably helps SGI1 to propagate efficiently between IncC$^+$ or IncA$^+$ cells. SGI1 also seems to exclude A/C plasmids by an unknown mechanism (30). Furthermore, SGI1 excises and replicates in the presence of a helper plasmid while destabilizing it (56, 57). SGI1 has recently been shown to coopt the ParAB partitioning system of IncC plasmids to ensure the proper segregation of its replicative

form in daughter cells, eliciting helper IncC plasmid loss (56, 60). By directly inhibiting IncC and IncA plasmid cotransfer via CtiC, SGI1-like IMEs add to the antagonism arsenal that curbs the spread of their helper plasmids on multiple fronts.

MATERIALS AND METHODS

Bacterial strains, plasmids, and media

The bacterial strains and plasmids used in this study are described in Supplemental Table 1.

Bacterial strains were grown at 37°C on Luria-Bertani (LB) agar or with agitation in LB broth.

Bacterial strains were maintained at −75°C in LB broth containing 20% (vol/vol) glycerol.

Antibiotics were used at the following concentrations: ampicillin (Ap), 100 µg/ml; kanamycin (Km), 50 µg/ml; spectinomycin (Sp) 50 µg/ml; rifampicin (Rf), 50 µg/ml; chloramphenicol (Cm), 20 µg/ml; nalidixic acid (Nx), 40 µg/ml; tetracycline (Tc), 12 µg/ml. For induction of gene expression, bacterial cultures were supplemented with 0.02% (wt/vol) L-arabinose or 1 mM isopropyl β-D-1-thiogalactopyranoside (IPTG). When necessary, LB agar was supplemented with 40 µg/ml 5-bromo-4-chloro-3-indolyl β-D-galactopyranoside (X-gal).

Conjugation assays

Except for the TraDIS experiment (see below), conjugation assays were performed by mixing equal volumes of of donor and recipient cultures grown at 37°C with shaking overnight (6-hour mating) or for 4 hours (2-h mating). The cells were harvested by centrifugation, washed in 1 volume of LB broth and resuspended in 1/20 volume of LB broth. The mixtures were then deposited on LB agar plates and incubated at 37°C for 2, 4, or 6 hours. After mating, the cells were recovered from the plates in 1 ml of LB broth, and serial dilutions were prepared in LB broth for immediate plating. Donors, recipients and transconjugants were selected on LB agar plates containing appropriate antibiotics. Frequencies of transfer were calculated by dividing the number of transconjugant CFUs by the number of donor CFUs. When required for induction of gene expression during complementation experiments, LB agar plates were supplemented with L-arabinose (0.02%, wt/vol).

Molecular biology methods

Genomic DNA and plasmid extraction was prepared using QIAamp DNA mini kit and QIAprep Spin miniprep kit (Qiagen) or Monarch Plasmid Miniprep Kit (New England Biolabs), respectively, according to the manufacturer's instructions. Restrictions enzymes, Antarctic Phosphatase and T4 DNA Ligase used in this study were purchased from New England Biolabs. Several DNA polymerases were used: Q5 (New England Biolabs), Taq (New England Biolabs) and Easy Taq (Civic Bioscience). PCR products were purified using the QIAquick PCR Purification Kit (Qiagen), according to manufacturer's instructions. *E. coli* was transformed by electroporation as described by Dower *et al.* (61) in a Bio-Rad GenePulser Xcell apparatus set at 25 µF, 200 Ω and 1.8kV using 1-mm electroporation cuvettes. Sanger sequencing reactions were performed by the Plateforme de Séquençage et de Génotypage du Centre de Recherche du CHUL (Québec, QC, Canada).

Plasmid and strain construction

Plasmids and oligonucleotides used in this study are listed in Table 1 and Supplementary Table S9. Deletion and insertion mutants were constructed using the one-step chromosomal gene inactivation technique of Datsenko and Wanner (62). All deletions were designed to be non-polar. *traHG* and tra_S deletion mutants of SGI1^{Km} were constructed previously (13). Details about constructs are provided in Supplemental Text 1.

Transposon-directed insertion sequencing (TraDIS)

A conjugation-assisted random transposon mutagenesis experiment was performed on *E. coli* KH95 bearing pVCR94^{Km} Δ*acr2 trmE*::SGI1^{Cm} using the transposition system of *E. coli* MFD*pir*+ carrying pFG036 and pFG051 as described previously (15). Details are provided in Supplemental Text 1.

Preparation of TraDIS libraries and Illumina sequencing

For each library, a 1.5 ml frozen stock aliquot was thawed on ice for 15 min and used to prepare sequencing libraries as described previously (15). Mutant libraries were then pooled and sequenced by Illumina using the NextSeq 500/550 High Output Kit v2 at the RNomics platform of the Laboratoire de Génomique Fonctionnelle de l'Université de Sherbrooke (https:// rnomics.med.usherbrooke.ca) (Sherbrooke, QC, Canada). The transposon data analysis was carried out as described previously (15).

Bacterial adenylate cyclase two-hybrid (BACTH) assays

Protein-protein interactions were examined using a bacterial two-hybrid assay based on the reconstitution of the adenylate cyclase CyaA of *Bordetella pertussis* from the fragment T18 and T25 expressed from the two BACTH vectors pUT18C and pKT25 (63). The plasmid constructs expressing the genes of interests were transformed into *E. coli* BTH101. CyaA activity was measured through the activation of the expression of the *lacZ* reporter gene.

β-galactosidase assays

β-galactosidase assays were carried out on LB agar plates supplemented with 40 µg/mL 5-bromo-4-chloro-3-indolyl-β-D-galactopyranoside (X-gal) and 0.5 mM isopropyl β-D-1-thiogalactopyranoside (IPTG) for 36h at room temperature or in LB broth using *o*-nitrophenyl-β-D-galactopyranoside (ONPG) as the substrate as described previously (64). Overnight cultures were diluted 1:100, and further grown to mid-log phase (OD_{600} = 0.6). The mean values and standard error of the mean of β-galactosidase activities were calculated from 3 independent experiments.

RNA extraction and cDNA synthesis

RNA extractions and cDNA synthesis were performed as previously described (21) with the following modifications. *E. coli* VB112 containing SGI1^{Km} with or without pBAD-*acaCD* was grown at 37°C for 16 h in LB broth containing the appropriate antibiotics. cDNA was

synthesized from 0.5 ng of RNA and 1 pmol of gene-specific primer ctiC_RT (Integrated DNA Technologies), using the reverse transcriptase SuperScript IV (Invitrogen), according to the manufacturer's instructions. Control reactions without reverse transcriptase treatment ('RNA') were performed for each sample. PCR reactions aiming at amplifying *traG-ctiC* and *traH* were carried out using 50 pg of RNA or the corresponding amount of cDNA, or 0.5 ng of gDNA as the template, and primer pairs traG_i_F2/ctiC_i_R and traH_i_F/traH_i_R, respectively.

Multiple sequence alignment for sequence comparison and phylogenetic analyses

Initial comparative analyses of CtiC were conducted with HHblits (https://toolkit.tuebingen.mpg.de/tools/hhblits) (65). The diversity of domain architectures of proteins related to CtiC was assessed with a PSI-Blast analysis of CtiC against the NCBI Protein Reference Sequences restricted to Gammaproteobacteria (5 iterations, taxid: 1236). The recovered sequences where clustered using mmseqs2 (https://toolkit.tuebingen.mpg.de/tools/mmseqs2) with a minimum sequence identity parameter set to 1 to remove redundant sequences (66). Multiple sequence alignments (MUSCLE), alignment curation (trimAl) and tree inference with model selection and bootstrap (PhyML +SMS) were conducted as a workflow on the https://ngphylogeny.fr/ server (67–72). Trees were displayed and annotated with iTOL (73).

Protein structure predictions

Modeling of protein structures was done using the Alphafold server (https://alphafoldserver.com/) with default parameters (74). The generated PDB files were visualized and analyzed using the ChimeraX 1.9 software (75). Structure similarity searches were performed by the protein structure comparison tools PDBeFold v2.58 (http://www.ebi.ac.uk/msd-srv/ssm) (76) and Dali (http://ekhidna2.biocenter.helsinki.fi/dali/) (77) against the whole PDB archive. All against all structure comparisons were computed on

the Dali server. Sequence similarities and secondary structure information from aligned sequences were rendered using ESPript 3.0 (https://espript.ibcp.fr) (78).

Statistical analyses and figures preparation

Numerical data presented in graphs are available in S3 Dataset. All analyses were performed using R Statistical Software (v4.2.1) and RStudio (v2022.7.2.576) (79). We assumed a normal distribution of the frequencies of transconjugant formation and tested the homogeneity of variance of the $\log_{10}$-transformed frequencies using Bartlett's tests. Dunnett and Tukey-Kramer tests and compact letter display were performed via the multcomp R package (v1.4-20) (80). Graphics were rendered via the ggplot2 (v3.3.6) (81) and pheatmap (v1.0.12) (82) R packages. All figures were prepared using Inkscape 1.4 (https://inkscape.org/).

DATA AVAILABILITY

Raw sequencing data of TraDIS experiments were submitted to Genbank Sequence Read Archive (SRA) under BioProject accession number PRJNA857050 with the following BioSample accession numbers: SAMN29603706 and SAMN29603707 for *E. coli* KH95 bearing pVCR94^{Km} Δ*acr2* and SGI1^{Cm} as the donor strain (input); SAMN29603708 and SAMN29603709 for transconjugants with *E. coli* GG56 as the recipient strain (output). Complete data from aligned reads can also be visualized using the UCSC genome browser at https://genome.ucsc.edu/cgi-bin/hgHubConnect?hgHub_do_redirect=on&hgHubConnect.remakeTrackHub=on&hgHub_do_firstDb=1&hubUrl=https://datahub-101-cw2.p.genap.ca/Deschenes_2023_SGI1Cm/SGI1Cm.hub.txt (SGI1^{Cm}) and https://genome.ucsc.edu/cgi-bin/hgHubConnect?hgHub_do_redirect=on&hgHubConnect.remakeTrackHub=on&hgHub_do_firstDb=1&hubUrl=https://datahub-101-cw2.p.genap.ca/Deschenes_2023_pVCR94dX3dacr2/pVCR94dX3dacr2.hub.txt (pVCR94^{Km} Δ*acr2*).

ACKNOWLEDGMENTS

We are grateful to Christian Baron for the kind gift of *E. coli* BTH101 and the BACTH plasmids pUT18C and pKT25, and their *zip* derivative. We also thank Benoît Doublet for the kind gift of the IncA conjugative plasmid pRA1 and Frédérik Leroux for technical assistance.

FUNDING

This work was supported by a Discovery Grant [RGPIN -202102814] from the Natural Sciences and Engineering Research Council of Canada (NSERC) and Project Grants [PJT-153071 and PJT-186081] from the Canadian Institutes of Health Research (CIHR) to V.B. R.D. received a Fonds de recherche du Québec-Nature et Technologies (FRQNT) doctoral

fellowship. K.T.H. was supported by a postdoctoral fellowship [SPE20170336797] from the Fondation de la Recherche Médicale (FRM, France). N.R. received an Alexander Graham Bell Canada Graduate Scholarship from the NSERC. The funders had no role in study design, data collection and interpretation, or the decision to submit the work for publication.

COMPETING INTERESTS

The authors have no competing interests to declare.

REFERENCES

1. Partridge SR, Kwong SM, Firth N, Jensen SO. 2018. Mobile Genetic Elements Associated with Antimicrobial Resistance. Clin Microbiol Rev 31:e00088-17.

2. Botelho J, Schulenburg H. 2021. The Role of Integrative and Conjugative Elements in Antibiotic Resistance Evolution. Trends Microbiol 29:8–18.

3. Castañeda-Barba S, Top EM, Stalder T. 2024. Plasmids, a molecular cornerstone of antimicrobial resistance in the One Health era. Nat Rev Microbiol 22:18–32.

4. Cabezón E, Ripoll-Rozada J, Peña A, Cruz F de la, Arechaga I. 2015. Towards an integrated model of bacterial conjugation. FEMS Microbiology Reviews 39:81–95.

5. Bellanger X, Payot S, Leblond-Bourget N, Guédon G. 2014. Conjugative and mobilizable genomic islands in bacteria: evolution and diversity. FEMS Microbiology Reviews 38:720–760.

6. Ares-Arroyo M, Coluzzi C, Moura de Sousa JA, Rocha EPC. 2024. Hijackers, hitchhikers, or co-drivers? The mysteries of mobilizable genetic elements. PLoS Biol 22:e3002796.

7. Harmer CJ, Hall RM. 2015. The A to Z of A/C plasmids. Plasmid 80:63–82.

8. Carraro N, Sauvé M, Matteau D, Lauzon G, Rodrigue S, Burrus V. 2014. Development of pVCR94ΔX from *Vibrio cholerae*, a prototype for studying multidrug resistant IncA/C conjugative plasmids. Front Microbiol 5:44.

9. Fricke WF, Welch TJ, McDermott PF, Mammel MK, LeClerc JE, White DG, Cebula TA, Ravel J. 2009. Comparative genomics of the IncA/C multidrug resistance plasmid family. J Bacteriol 191:4750–4757.

10. Ma L, Yin Z, Zhang D, Zhan Z, Wang Q, Duan X, Gao H, Liang Q, Zhao Y, Feng J, Zhao Y, Tong Y, Dai E, Zhou D. 2017. Comparative genomics of type 1 IncC plasmids from China. Future Microbiol 12:1511–1522.

11. Fernández-Alarcón C, Singer RS, Johnson TJ. 2011. Comparative genomics of multidrug resistance-encoding IncA/C plasmids from commensal and pathogenic *Escherichia coli* from multiple animal sources. PLoS One 6:e23415.

12. Hazen TH, Zhao L, Boutin MA, Stancil A, Robinson G, Harris AD, Rasko DA, Johnson JK. 2014. Comparative genomics of an IncA/C multidrug resistance plasmid from *Escherichia coli* and *Klebsiella* isolates from intensive care unit patients and the utility of whole-genome sequencing in health care settings. Antimicrob Agents Chemother 58:4814–4825.

13. Carraro N, Durand R, Rivard N, Anquetil C, Barrette C, Humbert M, Burrus V. 2017. *Salmonella* genomic island 1 (SGI1) reshapes the mating apparatus of IncC conjugative plasmids to promote self-propagation. PLOS Genetics 13:e1006705.

14. Carraro N, Matteau D, Luo P, Rodrigue S, Burrus V. 2014. The master activator of IncA/C conjugative plasmids stimulates genomic islands and multidrug resistance dissemination. PLoS Genet 10:e1004714.

15. Roy D, Huguet KT, Grenier F, Burrus V. 2020. IncC conjugative plasmids and SXT/R391 elements repair double-strand breaks caused by CRISPR-Cas during conjugation. Nucleic Acids Res 48:8815–8827.

16. Hancock SJ, Phan M-D, Luo Z, Lo AW, Peters KM, Nhu NTK, Forde BM, Whitfield J, Yang J, Strugnell RA, Paterson DL, Walsh TR, Kobe B, Beatson SA, Schembri MA. 2020. Comprehensive analysis of IncC plasmid conjugation identifies a crucial

role for the transcriptional regulator AcaB. Nat Microbiol 5:1340–1348.

17. Hancock SJ, Phan M-D, Peters KM, Forde BM, Chong TM, Yin W-F, Chan K-G, Paterson DL, Walsh TR, Beatson SA, Schembri MA. 2017. Identification of IncA/C Plasmid Replication and Maintenance Genes and Development of a Plasmid Multilocus Sequence Typing Scheme. Antimicrob Agents Chemother 61:e01740-16.

18. Hancock SJ, Phan M, Roberts LW, Vu TNM, Harris PNA, Beatson SA, Schembri MA. 2021. Characterization of DtrJ as an IncC plasmid conjugative DNA transfer component. Mol Microbiol 116:154–167.

19. Hegyi A, Szabó M, Olasz F, Kiss J. 2017. Identification of *oriT* and a recombination hot spot in the IncA/C plasmid backbone. Sci Rep 7:10595.

20. Humbert M, Huguet KT, Coulombe F, Burrus V. 2019. Entry Exclusion of Conjugative Plasmids of the IncA, IncC, and Related Untyped Incompatibility Groups. J Bacteriol 201:e00731-18.

21. Rivard N, Humbert M, Huguet KT, Fauconnier A, Bucio CP, Quirion E, Burrus V. 2024. Surface exclusion of IncC conjugative plasmids and their relatives. PLoS Genet 20:e1011442.

22. Douard G, Praud K, Cloeckaert A, Doublet B. 2010. The *Salmonella* genomic island 1 is specifically mobilized in trans by the IncA/C multidrug resistance plasmid family. PLoS ONE 5:e15302.

23. Carraro N, Rivard N, Ceccarelli D, Colwell RR, Burrus V. 2016. IncA/C Conjugative Plasmids Mobilize a New Family of Multidrug Resistance Islands in Clinical *Vibrio*

cholerae Non-O1/Non-O139 Isolates from Haiti. mBio 7:e00509-16.

24. Boyd D, Peters GA, Cloeckaert A, Boumedine KS, Chaslus-Dancla E, Imberechts H, Mulvey MR. 2001. Complete nucleotide sequence of a 43-kilobase genomic island associated with the multidrug resistance region of *Salmonella enterica* serovar Typhimurium DT104 and its identification in phage type DT120 and serovar Agona. J Bacteriol 183:5725–5732.

25. de Curraize C, Siebor E, Neuwirth C. 2021. Genomic islands related to *Salmonella* genomic island 1; integrative mobilisable elements in *trmE* mobilised in trans by A/C plasmids. Plasmid 114:102565.

26. Durand R, Deschênes F, Burrus V. 2021. Genomic islands targeting *dusA* in *Vibrio* species are distantly related to *Salmonella* Genomic Island 1 and mobilizable by IncC conjugative plasmids. PLoS Genet 17:e1009669.

27. Kiss J, Szabó M, Hegyi A, Douard G, Praud K, Nagy I, Olasz F, Cloeckaert A, Doublet B. 2019. Identification and Characterization of *oriT* and Two Mobilization Genes Required for Conjugative Transfer of *Salmonella* Genomic Island 1. Front Microbiol 10:457.

28. Harmer CJ, Hamidian M, Ambrose SJ, Hall RM. 2016. Destabilization of IncA and IncC plasmids by SGI1 and SGI2 type *Salmonella* genomic islands. Plasmid 87–88:51–57.

29. Ambrose SJ, Hall RM. 2022. Can SGI1 family integrative mobilizable elements overcome entry exclusion exerted by IncA and IncC plasmids on IncC plasmids? Plasmid 123–124:102654.

30. Ambrose SJ, Hall RM. 2025. SGI1 excludes IncA and IncC plasmids. Plasmid 133:102743.

31. Getino M, de la Cruz F. 2018. Natural and Artificial Strategies To Control the Conjugative Transmission of Plasmids. Microbiol Spectr 6:6.1.03.

32. Cabezón E, Sastre JI, de la Cruz F. 1997. Genetic evidence of a coupling role for the TraG protein family in bacterial conjugation. Mol Gen Genet 254:400–406.

33. Núñez B, De La Cruz F. 2001. Two atypical mobilization proteins are involved in plasmid CloDF13 relaxation. Mol Microbiol 39:1088–1099.

34. Yan J, Beattie TR, Rojas AL, Schermerhorn K, Gristwood T, Trinidad JC, Albers SV, Roversi P, Gardner AF, Abrescia NGA, Bell SD. 2017. Identification and characterization of a heterotrimeric archaeal DNA polymerase holoenzyme. Nat Commun 8:15075.

35. Aravind L, Anantharaman V, Balaji S, Babu M, Iyer L. 2005. The many faces of the helix-turn-helix domain: Transcription regulation and beyond. FEMS Microbiology Reviews 29:231–262.

36. Gajiwala KS, Burley SK. 2000. Winged helix proteins. Current Opinion in Structural Biology 10:110–116.

37. de Curraize C, Siebor E, Varin V, Neuwirth C, Hall RM. 2020. Two New SGI1-LK Variants Found in *Proteus mirabilis* and Evolution of the SGI1-HKL Group of *Salmonella* Genomic Islands. mSphere 5:e00875-19.

38. Durand R, Huguet KT, Rivard N, Carraro N, Rodrigue S, Burrus V. 2021. Crucial role of *Salmonella* genomic island 1 master activator in the parasitism of IncC

plasmids. Nucleic Acids Res 49:7807–7824.

39. Koraimann G, Teferle K, Markolin G, Woger W, Högenauer G. 1996. The FinOP repressor system of plasmid R1: analysis of the antisense RNA control of *traJ* expression and conjugative DNA transfer. Molecular Microbiology 21:811–821.

40. Gasson MJ, Willetts NS. 1977. Further characterization of the F fertility inhibition systems of “unusual” Fin+ plasmids. J Bacteriol 131:413–420.

41. Gaffney D, Skurray R, Willetts N, Brenner S. 1983. Regulation of the F conjugation genes studied by hybridization and *tra-lacZ* fusion. Journal of Molecular Biology 168:103–122.

42. Gasson MJ, Willetts NS. 1975. Five control systems preventing transfer of *Escherichia coli* K-12 sex factor F. J Bacteriol 122:518–525.

43. Willetts N. 1980. Interactions between the F conjugal transfer system and CloDF13::TnA plasmids. Molec Gen Genet 180:213–217.

44. Santini JM, Stanisich VA. 1998. Both the *fipA* gene of pKM101 and the *pifC* gene of F inhibit conjugal transfer of RP1 by an effect on *traG*. J Bacteriol 180:4093–4101.

45. Maindola P, Raina R, Goyal P, Atmakuri K, Ojha A, Gupta S, Christie PJ, Iyer LM, Aravind L, Arockiasamy A. 2014. Multiple enzymatic activities of ParB/Srx superfamily mediate sexual conflict among conjugative plasmids. Nat Commun 5:5322.

46. Ceccarelli D, Daccord A, René M, Burrus V. 2008. Identification of the origin of transfer (*oriT*) and a new gene required for mobilization of the SXT/R391 family of integrating conjugative elements. J Bacteriol 190:5328–5338.

47. Wisniewski JA, Traore DA, Bannam TL, Lyras D, Whisstock JC, Rood JI. 2016. TcpM: a novel relaxase that mediates transfer of large conjugative plasmids from *Clostridium perfringens*: The novel relaxase TcpM. Molecular Microbiology 99:884–896.

48. Garcillán-Barcia MP, Francia MV, de la Cruz F. 2009. The diversity of conjugative relaxases and its application in plasmid classification. FEMS Microbiol Rev 33:657–687.

49. Guzmán-Herrador DL, Llosa M. 2019. The secret life of conjugative relaxases. Plasmid 104:102415.

50. Soler N, Robert E, Chauvot De Beauchêne I, Monteiro P, Libante V, Maigret B, Staub J, Ritchie DW, Guédon G, Payot S, Devignes M-D, Leblond-Bourget N. 2019. Characterization of a relaxase belonging to the MOBT family, a widespread family in Firmicutes mediating the transfer of ICEs. Mobile DNA 10:18.

51. Heilers J-H, Reiners J, Heller E-M, Golzer A, Smits SHJ, van der Does C. 2019. DNA processing by the MOB_H family relaxase TraI encoded within the gonococcal genetic island. Nucleic Acids Res 47:8136–8153.

52. Lawley TD, Gilmour MW, Gunton JE, Standeven LJ, Taylor DE. 2002. Functional and mutational analysis of conjugative transfer region 1 (Tra1) from the IncHI1 plasmid R27. J Bacteriol 184:2173–2180.

53. Rivard N, Colwell RR, Burrus V. 2020. Antibiotic Resistance in *Vibrio cholerae*: Mechanistic Insights from IncC Plasmid-Mediated Dissemination of a Novel Family of Genomic Islands Inserted at *trmE*. mSphere 5:e00748-20.

54. Pons MC, Praud K, Da Re S, Cloeckaert A, Doublet B. 2022. Conjugative IncC Plasmid Entry Triggers the SOS Response and Promotes Effective Transfer of the Integrative Antibiotic Resistance Element SGI1. Microbiol Spectr e02201-22.

55. Kiss J, Nagy B, Olasz F. 2012. Stability, entrapment and variant formation of *Salmonella* genomic island 1. PLoS ONE 7:e32497.

56. Huguet KT, Rivard N, Garneau D, Palanee J, Burrus V. 2020. Replication of the *Salmonella* Genomic Island 1 (SGI1) triggered by helper IncC conjugative plasmids promotes incompatibility and plasmid loss. PLoS Genet 16:e1008965.

57. Szabó M, Murányi G, Kiss J. 2021. IncC helper dependent plasmid-like replication of *Salmonella* Genomic Island 1. Nucleic Acids Research 49:832–846.

58. Grim CJ, Hasan NA, Taviani E, Haley B, Chun J, Brettin TS, Bruce DC, Detter JC, Han CS, Chertkov O, Challacombe J, Huq A, Nair GB, Colwell RR. 2010. Genome sequence of hybrid *Vibrio cholerae* O1 MJ-1236, B-33, and CIRS101 and comparative genomics with *V. cholerae*. J Bacteriol 192:3524–3533.

59. Weill F-X, Domman D, Njamkepo E, Tarr C, Rauzier J, Fawal N, Keddy KH, Salje H, Moore S, Mukhopadhyay AK, Bercion R, Luquero FJ, Ngandjio A, Dosso M, Monakhova E, Garin B, Bouchier C, Pazzani C, Mutreja A, Grunow R, Sidikou F, Bonte L, Breurec S, Damian M, Njanpop-Lafourcade B-M, Sapriel G, Page A-L, Hamze M, Henkens M, Chowdhury G, Mengel M, Koeck J-L, Fournier J-M, Dougan G, Grimont PAD, Parkhill J, Holt KE, Piarroux R, Ramamurthy T, Quilici M-L, Thomson NR. 2017. Genomic history of the seventh pandemic of cholera in Africa. Science 358:785–789.

60. Murányi G, Szabó M, Acsai K, Kiss J. 2024. Two birds with one stone: SGI1 can

stabilize itself and expel the IncC helper by hijacking the plasmid *parABS* system. Nucleic Acids Research gkae050.

61. Dower WJ, Miller JF, Ragsdale CW. 1988. High efficiency transformation of *E. coli* by high voltage electroporation. Nucleic Acids Res 16:6127–6145.

62. Datsenko KA, Wanner BL. 2000. One-step inactivation of chromosomal genes in *Escherichia coli* K-12 using PCR products. Proc Natl Acad Sci U S A 97:6640–6645.

63. Karimova G, Dautin N, Ladant D. 2005. Interaction Network among *Escherichia coli* Membrane Proteins Involved in Cell Division as Revealed by Bacterial Two-Hybrid Analysis. J Bacteriol 187:2233–2243.

64. Miller JH. 1992. A Short Course in Bacterial Genetics: A Laboratory Manual and Handbook for *Escherichia coli* and Related Bacteria. Cold Spring Harbor Laboratory Press, Cold Spring Harbor.

65. Remmert M, Biegert A, Hauser A, Söding J. 2012. HHblits: lightning-fast iterative protein sequence searching by HMM-HMM alignment. Nat Methods 9:173–175.

66. Mirdita M, Steinegger M, S"oding J. 2019. MMseqs2 desktop and local web server app for fast, interactive sequence searches. Bioinformatics 35:2856–2858.

67. Lemoine F, Correia D, Lefort V, Doppelt-Azeroual O, Mareuil F, Cohen-Boulakia S, Gascuel O. 2019. NGPhylogeny.fr: new generation phylogenetic services for non-specialists. Nucleic Acids Research 47:W260–W265.

68. Capella-Gutiérrez S, Silla-Martínez JM, Gabaldón T. 2009. trimAl: a tool for automated alignment trimming in large-scale phylogenetic analyses. Bioinformatics

25:1972–1973.

69. Edgar RC. 2004. MUSCLE: multiple sequence alignment with high accuracy and high throughput. Nucleic Acids Res 32:1792–1797.

70. Guindon S, Dufayard J-F, Lefort V, Anisimova M, Hordijk W, Gascuel O. 2010. New algorithms and methods to estimate maximum-likelihood phylogenies: assessing the performance of PhyML 3.0. Syst Biol 59:307–321.

71. Lefort V, Longueville J-E, Gascuel O. 2017. SMS: Smart Model Selection in PhyML. Molecular Biology and Evolution 34:2422–2424.

72. Lemoine F, Domelevo Entfellner J-B, Wilkinson E, Correia D, Dávila Felipe M, De Oliveira T, Gascuel O. 2018. Renewing Felsenstein's phylogenetic bootstrap in the era of big data. Nature 556:452–456.

73. Letunic I, Bork P. 2024. Interactive Tree of Life (iTOL) v6: recent updates to the phylogenetic tree display and annotation tool. Nucleic Acids Research 52:W78–W82.

74. Abramson J, Adler J, Dunger J, Evans R, Green T, Pritzel A, Ronneberger O, Willmore L, Ballard AJ, Bambrick J, Bodenstein SW, Evans DA, Hung C-C, O'Neill M, Reiman D, Tunyasuvunakool K, Wu Z, Žemgulytė A, Arvaniti E, Beattie C, Bertolli O, Bridgland A, Cherepanov A, Congreve M, Cowen-Rivers AI, Cowie A, Figurnov M, Fuchs FB, Gladman H, Jain R, Khan YA, Low CMR, Perlin K, Potapenko A, Savy P, Singh S, Stecula A, Thillaisundaram A, Tong C, Yakneen S, Zhong ED, Zielinski M, Žídek A, Bapst V, Kohli P, Jaderberg M, Hassabis D, Jumper JM. 2024. Accurate structure prediction of biomolecular interactions with AlphaFold 3. Nature 630:493–500.

75. Goddard TD, Huang CC, Meng EC, Pettersen EF, Couch GS, Morris JH, Ferrin TE. 2018. UCSF ChimeraX: Meeting modern challenges in visualization and analysis: UCSF ChimeraX Visualization System. Protein Science 27:14–25.

76. Krissinel E, Henrick K. 2004. Secondary-structure matching (SSM), a new tool for fast protein structure alignment in three dimensions. Acta Crystallogr D Biol Crystallogr 60:2256–2268.

77. Holm L. 2022. Dali server: structural unification of protein families. Nucleic Acids Research 50:W210–W215.

78. Robert X, Gouet P. 2014. Deciphering key features in protein structures with the new ENDscript server. Nucleic Acids Research 42:W320–W324.

79. R Core Team. 2022. R: A Language and Environment for Statistical Computing. R Foundation for Statistical Computing, Vienna, Austria. https://www.R-project.org/.

80. Hothorn T, Bretz F, Westfall P. 2008. Simultaneous Inference in General Parametric Models. Biom J 50:346–363.

81. Wickham H. 2016. ggplot2: Elegant Graphics for Data Analysis. Springer-Verlag New York. https://ggplot2.tidyverse.org.

82. Kolde R. 2018. pheatmap: Pretty Heatmaps. https://github.com/raivokolde/pheatmap.

83. Ferrières L, Hémery G, Nham T, Guérout A-M, Mazel D, Beloin C, Ghigo J-M. 2010. Silent mischief: bacteriophage Mu insertions contaminate products of *Escherichia coli* random mutagenesis performed using suicidal transposon delivery plasmids mobilized by broad-host-range RP4 conjugative machinery. J Bacteriol

192:6418–6427.

84. Grenier F, Matteau D, Baby V, Rodrigue S. 2014. Complete genome sequence of *Escherichia coli* BW25113. Genome Announc 2:pii: e01038-14.

85. Singer M, Baker TA, Schnitzler G, Deischel SM, Goel M, Dove W, Jaacks KJ, Grossman AD, Erickson JW, Gross CA. 1989. A collection of strains containing genetically linked alternating antibiotic resistance elements for genetic mapping of *Escherichia coli*. Microbiol Rev 53:1–24.

86. Garriss G, Waldor MK, Burrus V. 2009. Mobile antibiotic resistance encoding elements promote their own diversity. PLoS Genet 5:e1000775.

87. Datta S, Costantino N, Court DL. 2006. A set of recombineering plasmids for gram-negative bacteria. Gene 379:109–115.

88. Cherepanov PP, Wackernagel W. 1995. Gene disruption in *Escherichia coli*: TcR and KmR cassettes with the option of Flp-catalyzed excision of the antibiotic-resistance determinant. Gene 158:9–14.

89. Aoki T, Egusa S, Ogata Y, Watanabe T. 1971. Detection of Resistance Factors in Fish Pathogen *Aeromonas liquefaciens*. Journal of General Microbiology 65:343–349.

90. Guzman LM, Belin D, Carson MJ, Beckwith J. 1995. Tight regulation, modulation, and high-level expression by vectors containing the arabinose P_{BAD} promoter. J Bacteriol 177:4121–4130.

91. Karimova G, Ullmann A, Ladant D. 2001. Protein-protein interaction between *Bacillus stearothermophilus* tyrosyl-tRNA synthetase subdomains revealed by a

bacterial two-hybrid system. J Mol Microbiol Biotechnol 3:73–82.

92. Karimova G, Ullmann A, Ladant D. 2000. A bacterial two-hybrid system that exploits a cAMP signaling cascade in *Escherichia coli*, p. 59–73. *In* Methods in Enzymology. Elsevier.

Table 1. Strains, plasmids and IMEs used in this study

Strain, plasmid or IME	Relevant genotype, phenotype or description[a]	Reference or source
***E. coli* strains**		
MG1655	K-12 F^- λ^- *ilvG*$^-$ *rfb-50 rph-1*	CGSC#6300
VB112	Rf-derivative of MG1655 (Rf)	(46)
MFD*pir*+	MG1655 RP4-2-Tc::[ΔMu1*::aac(3)IV*-Δ*aphA*-Δ*nic35*-ΔMu2::*zeo*] Δ*dapA::(erm-pir)* Δ*recA*	(83)
BW25113	F^- Δ(*araD-araB*)*567*, Δ*lacZ4787*(::*rrnB-3*), λ^-, *rph-1*, Δ(*rhaD-rhaB*)*568*, *hsdR514*	(62)
KH95	BW25113 *rpoB526* (Rf)	(56)
GG56	Nx-derivative of BW25113 (Nx)	(8, 84)
BTH101	F- *cya-99*, *araD139*, *galE15*, *galK16*, *rpsL1*, *hsdR2*, *mcrA1*, *mcrB1* (Sm)	(63)
CAG18349	MG1655 *lacZU118* (Lac-) *lacI42*::Tn*10* (Tc)	(85)
Plasmids		
pFG036	ori_{pMB1}, *cI857* (Ts) repressor, *tetM* (Tc)	Addgene #137996
pFG051	ori_{R6K}, tnp_{Tn5} under λP_L promoter, $oriT_{RP4}$, Tn*5d-aadA7* (Sp)	Addgene #137997
pKD3	Cm template for one-step chromosomal gene inactivation	(62)
pKD4	Km template for one-step chromosomal gene inactivation	(62)
pVI36	Sp template for one-step chromosomal gene inactivation	(46)
pVI42B	pVI36 BamHI::P_{lac}-*lacZ* (Sp)	(86)
pSIM6	λRed recombination thermo-inductible encoding plasmid (ts, Ap)	(87)
pSIM19	λRed recombination thermo-inductible encoding plasmid (ts, Sp)	(87)
pCP20	FLP recombinase thermo-inductible encoding plasmid (ts, Ap, Cm)	(88)
pRA1	IncA conjugative plasmid from *Aeromonas hydrophila* (Tc Su)	(89)
pVCR94	IncC conjugative plasmid from *V. cholerae* O1 El Tor (Su Tm Cm Ap Tc Sm)	(8)
pVCR94^{Sp}	Sp-derivative of pVCR94 (Sp Su)	(8)
pVCR94^{Km}	Km-derivative of pVCR94 (Km Su)	(8)
pVCR94^{Cm}	Cm-derivative of pVCR94 (Km Su)	(13)
pVCR94^{Km} Δ*acr2*	*acr2* deletion mutant of pVCR94^{Km} (Km Su)	This study
pVCR94^{Cm} *mobI-lacZ*	pVCR94^{Cm} expressing a translational fusion of the 8th codon of *lacZ* at the 5th codon of *mobI*	This study
pVCR94^{Cm} *traI-lacZ*	pVCR94^{Cm} expressing a translational fusion of the 8th codon of *lacZ* at the 5th codon of *traI*	This study
pVCR94^{Cm} *traI*ΔMIBD	Deletion mutant of pVCR94^{Cm} expressing *traI* lacking the MIBD domain (Cm Su)	This study
pVCR94^{Cm} *traI*ΔMIBD-*ctiC*	Mutant of pVCR94^{Cm} expressing *traI* with the MIBD domain (amino acid 900-986) replaced by *ctiC* (amino acid 2-83)	This Study
pSU4628	CloDF13::Tn*A*ΔEcoRV, $rep_{CloDF13}$, *mobBC* (Ap)	(32)
pBAD30	ori_{p15A} *araC* P_{BAD} (Ap)	(90)
pBAD-*acaCD*	pBAD30::*acaCD* (Ap)	(14)
pUC57-*ctiC*2	pUC57 with *ctiC* from IE*Vch*USA2 obtained by DNA synthesis (Bio Basic) (Km)	This study

pUC57-*unk*	pUC57 with the unknown *ctiC* from IE*Vch*USA5 obtained by DNA synthesis (Bio Basic (Km)	This study
pBAD-*ctiC*	*ctiC* of SGI1 cloned into EcoRI of pBAD30 (Ap)	This study
pBAD-*ctiC*2	*ctiC2* of IE*Vch*USA2 cloned into EcoRI of pBAD30 (Ap)	This study
pBAD-*ctiC*3	*ctiC3* of IME*Vch*USA3 cloned into EcoRI of pBAD30 (Ap)	This study
pBAD-*unk*	*unk* of IE*Vch*USA5 cloned into EcoRI of pBAD30 (Ap)	This study
pUT18C	pUC19 derivative; P_{lac}-*t18* (N-terminal T18 fragment [amino acid 225-399 of *B. pertussis* CyaA]) (Ap)	(91)
pKT25	pSU40 derivative; P_{lac}-*t25* (N-terminal T25 fragment [amino acid 1-224 of *B. pertussis* CyaA]) (Km)	(91)
pKT25-*ctiC*	*ctiC* of SGI1 cloned into pKT25 (EcoRI/XbaI) (Ap)	This study
pUT18C-c*tiC*	*ctiC* of SGI1 cloned into pUT18C (EcoRI/XbaI) (Ap)	This study
pKT25-*mobI*	*mobI* of pVCR94 cloned into pKT25 (EcoRI/XbaI) (Ap)	This study
pUT18C-*mobI*	*mobI* of pVCR94 cloned into pUT18C (EcoRI/XbaI) (Ap)	This study
pKT25-*traI*ΔHD	C-terminal half (amino acid 421-992) of *traI* of pVCR94 cloned into pKT25 (EcoRI/XbaI) (Ap)	This study
pUT18C-*traI*ΔHD	C-terminal half (amino acid 421-992) of *traI* of pVCR94 cloned into pUT18C (EcoRI/XbaI) (Ap)	This study
pKT25-*zip*	pKT25 with the leucine zipper domain of GCN4	(92)
pUT18C-*zip*	pUT18C with the leucine zipper domain of GCN4	(92)
pUT18C-*traI*ΔX	pUT18C-*traI*ΔHD lacking amino acid residues 654 to 766 (deletion of the X domain)	This study
pUT18C-*traI*Δ1	pUT18C-*traI*ΔHD lacking amino acid residues 2 to 653 (deletion of the Dis1 domain)	This study
pUT18C-*traI*Δ1-X	pUT18C-*traI*ΔHD lacking amino acid residues 2 to 766 (deletion of Dis1 and X domains)	This study
pUT18C-*traI*Δ1-X-2	pUT18C-*traI*ΔHD lacking amino acid residues 2 to 900 (deletion of Dis1, X, and Dis2 domains)	This study
pUT18C-*traI*ΔX-2-MIBD	pUT18C-*traI*ΔHD lacking amino acid residues 654 to 922 (deletion of X, Dis2, and MIBD domains)	This study
pUT18C-*traI*Δ2-MIBD	pUT18C-*traI*ΔHD lacking amino acid residues 777 to 922 (deletion of Dis2 and MIBD domains)	This study
pUT18C-*traI*ΔMIBD	pUT18C-*traI*ΔHD lacking amino acid residues 901 to 992 (deletion of the MIBD domain)	This study
pREDCas9	Constitutive expression of Cas9 and inducible expression of the λRed recombineering system (Ap)	Addgene #71541
pAC018	Expression of gRNA in *E. coli*	Addgene pending
pAC018ΔR::*aph*	Expression of a gRNA targeting the *aph* gene of pKD4	This study
IMEs		
SGI1^{Km}	ΔIn104::*aph* mutant of SGI1 lacking the integron In104 (Km)	(13)
SGI1^{Cm}	ΔIn104::*cat* mutant of SGI1 lacking the integron In104 (Cm)	(56)
SGI1^{Km} Δ*ctiC*	Δ*ctiC* (S010 ORF deleted) mutant of SGI1^{Km} (Km)	This study
SGI1^{Cm} Δ*ctiC*	Δ*ctiC* (S010 ORF deleted) mutant of SGI1^{Cm} (Cm)	This study
SGI1^{Km} Δ*HG*	Δ*traHG*$_S$ mutant of SGI1^{Km} (Km)	(13)
SGI1^{Km} Δ*HG* Δ*ctiC*	Δ*traHG*$_S$ Δ*ctiC* mutant of SGI1^{Km} (Km)	This study
SGI1^{Km} Δ*tra*$_s$	Δ(*traH-traN*) mutant of SGI1^{Km} (Km)	(13)
SGI1^{Km} *ctiC-lacZ*	SGI1^{Km} expressing a translational fusion of the 8th codon of *lacZ* at the 5th codon of *ctiC*	This study
IME*Vch*USA3^{Km}	Km-derivative of IME*Vch*USA3 (Km)	(26)
IME*Vch*USA3^{Km}	Δ*ctiC* mutant of IME*Vch*USA3^{Km} (Km)	This study

Δ*ctiC*		
IME*Vch*USA3^{Km} *ctiC-lacZ*	USA3^{Km} expressing a translational fusion of the 8th codon of *lacZ* at the 5th codon of *ctiC*	This study

[a] Ap, Ampicillin ; Cm, Chloramphenicol ; Km, Kanamycin; Nx, Nalidixic acid ; Rf, Rifampicin; Sm, Streptomycin ; Sp, Spectinomycin; Su, Sulfamethoxazole; Tc, Tetracycline; Ts, Thermo-sensitive

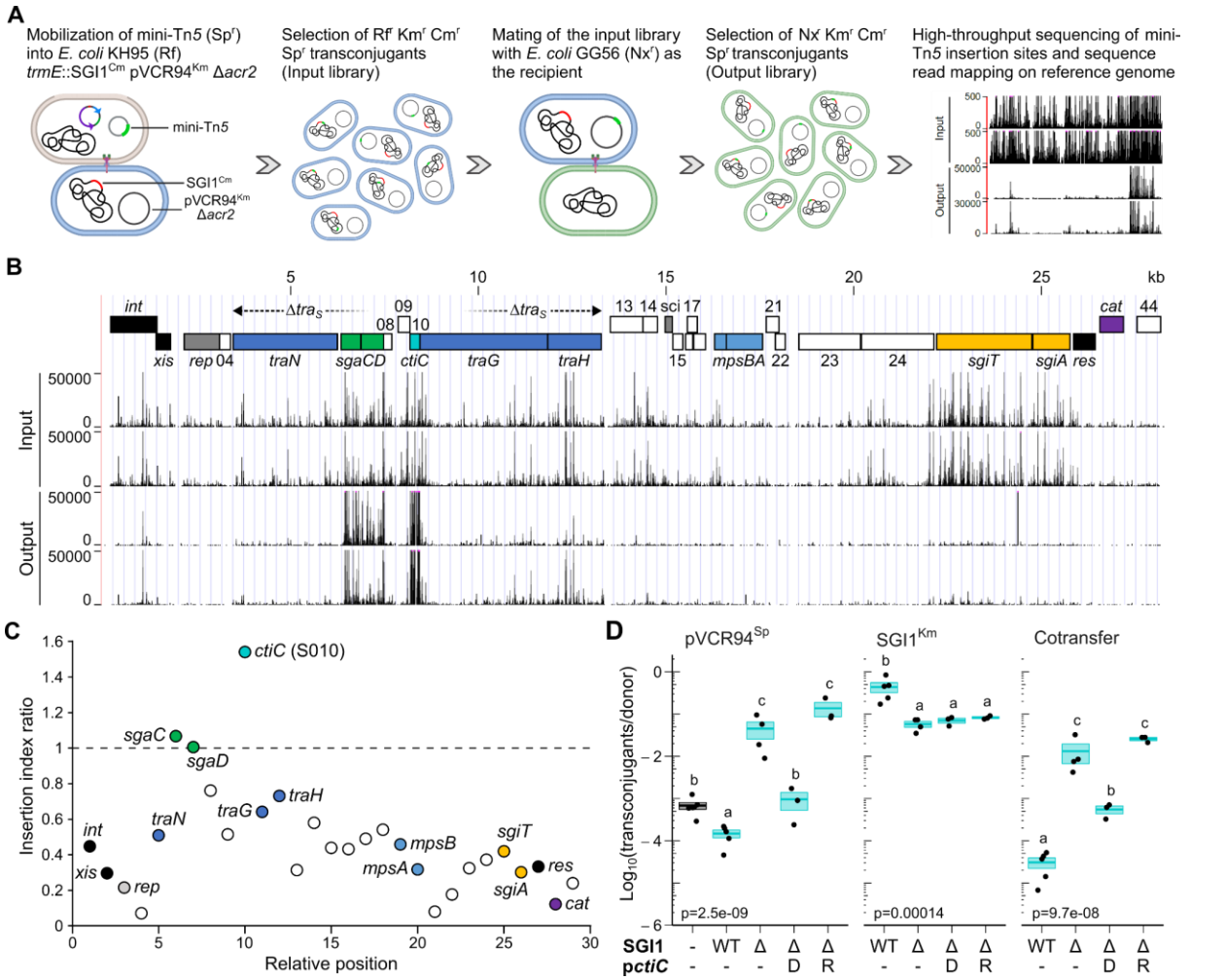

Figure 1. Identification of genes involved the inhibition in IncC plasmid transfer by high-density transposon mutagenesis. (**A**) TraDIS strategy for identifying genes that inhibit the cotransfer of SGI1 and its helper IncC plasmids in recipients. Created with BioRender.com. (**B**) Read mapping of mini-Tn*5* insertions in SGI1 in *E. coli* KH95 (Rf^r) bearing pVCR94^{Km} Δ*acr2* *trmE*::SGI1^{Cm} (Input) and in *E. coli* GG56 (Nx^r) transconjugants selected for cotransfer of pVCR94^{Km} and SGI1^{Cm} (Output). Genes on the map of SGI1^{Cm} (top track) are colour-coded as follows: black, recombination and transposition; dark grey, replication/partition; dark blue, mating pair formation; light blue, DNA processing; green, transcriptional activator; red, transcriptional repressor; yellow, toxin-antitoxin system; purple, antibiotic resistance; white, unknown function. In the input and output, each track corresponds to a biological replicate. (**C**) Dot plot of mini-Tn*5*

insertion index for each gene (S0xx) of SGI1^{Cm}. Insertion indexes were calculated as the ratios of insertion counts between input and output. (**D**) Effect of *ctiC* (S010) on the conjugative transfer of pVCR94^{Sp}. For all mating assays, *E. coli* GG56 (Nx^{r}) containing pVCR94^{Sp} was used as the donor strain, and *E. coli* CAG18439 (Tc^{r}) was used as the recipient strain. When indicated, the donor strain harboured SGI1^{Km} (WT) or its Δ*ctiC* mutant (Δ) with or without pBAD-*ctiC* (p*ctiC*). Expression of *ctiC* from pBAD30 in donor (D) or recipient (R) cells was induced with 0.02% arabinose. Crossbars show the mean and standard errors of the mean of at least three independent experiments. One-way ANOVA with a Tukey-Kramer post-test was used on the $\log_{10}$-transformed values to compare the means. The compact letter display shows statistical significance for pairwise comparisons, where means grouped under identical letters are not statistically different. The complete set of P values is presented in Table S1.

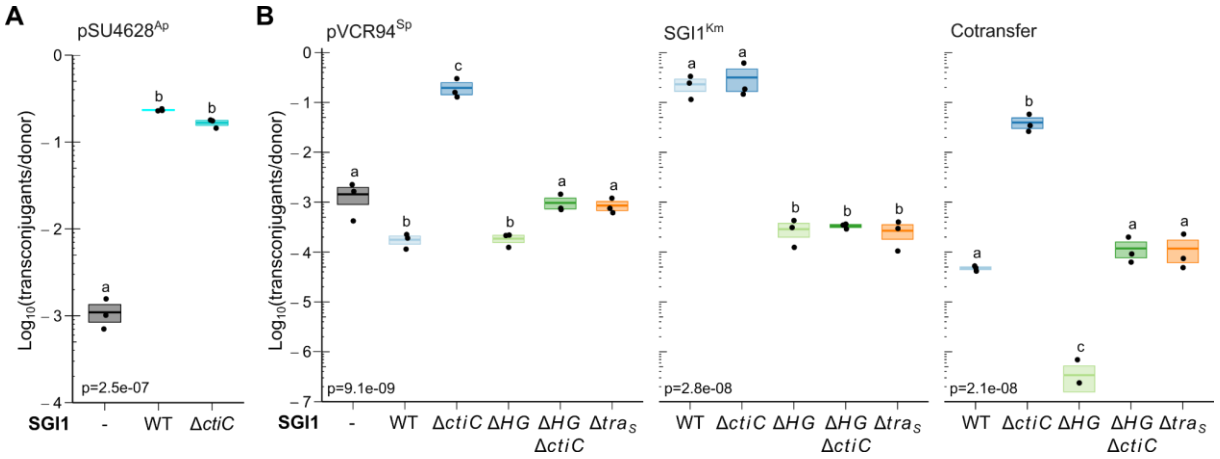

Figure 2. Effect of SGI1 and *ctiC* on conjugative transfer. (**A**) Effect of SGI1 and CtiC on the mobilization of pSU4628. *E. coli* GG56 (Nx^r) containing pVCR94^{Sp} and pSU4628^{Ap} was used as the donor strain. (**B**) Effect of *traHG* of SGI1 on IncC plasmid transfer in the presence or absence of *ctiC*. *E. coli* GG56 (Nx^r) containing pVCR94^{Sp} was used as the donor strain. In (A) and (B), *E. coli* CAG18439 (Tc^r) was used as the recipient strain, and when indicated, the donor harboured SGI1^{Km} (WT) or the designated SGI1^{Km} mutant. Transconjugants were selected as the Tc^r Ap^r (pSU4828), Tc^r Sp^r (pVCR94), Tc^r Km^r (SGI1), or Tc^r Sp^r Km^r (Cotransfer) colonies. Crossbars show the mean and standard errors of the mean of three independent experiments. Statistical treatment is as described in Fig. 1D. The complete set of P values is presented in Table S2.

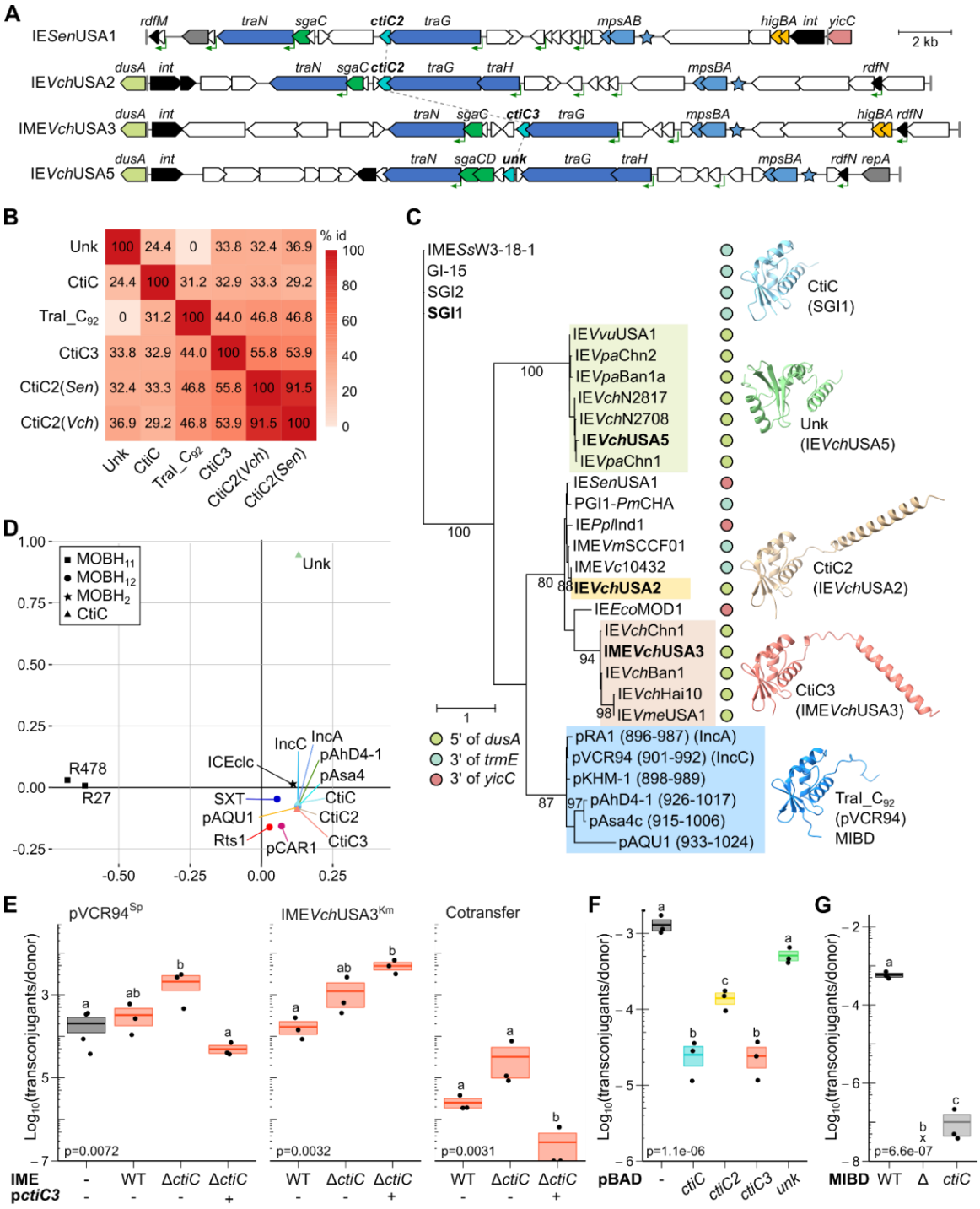

Figure 3. CtiC-related proteins or domains. (**A**) Genetic maps of IE*Sen*USA1 (*S. enterica* Kentucky ARS-CC8289; Genbank NZ_MCPS01000044), IME*Vch*USA3 (*V. cholerae* OYP6G08; Genbank NZ_NMSY01000009), IE*Vch*USA2 (*V. cholerae* 692–79; Genbank MIPA01000024), and IE*Vch*USA5 (*V. cholerae* OYP2C05; Genbank NZ_NMTM01000021). Colour keys are

indicated in Fig. 1. Green angled arrows indicate AcaCD-responsive promoters. (**B**) Pairwise comparison heatmap of blastp identity percentages of CtiC homologues and the last 92 amino acid residues of TraI (TraI_C_{92}) of pVCR94. Proteins accession numbers are as follows: CtiC (AAK38390.1), CtiC3 (WP_095463402.1), CtiC2(*Vch*) (OFI96794.1), CtiC2(*Sen*) (WP_069140155.1), Unk (WP_095467696.1), TraI_C_{92} (WP_011872892.1). (**C)** Maximum likelihood phylogenetic analysis of CtiC homologues. Bootstrap supports are indicated as percentages at the branching points only when >80%. Branch lengths represent the number of substitutions per site over 83 sites using the HIVb substitution model +G. Colored disks indicate IME's integration sites. Pink, yellow, and green backgrounds indicate *dusA*-integrated IMEs of type 1, 2, and 3, respectively, as defined elsewhere (26). CtiC proteins within the following clusters are identical: type 2 IE*Vch*USA2 (IE*Vch*Swe1 and GI*Vch*O27-1), type 1 IME*Vch*USA3 (IE*Vch*Aus1 and IE*Vch*N2786), and GI-15 (PGI2, AGI1, AGI1-B, and KGI1). The lineage with the blue background contains relaxase CTDs with TraI_C_{92} predicted structure used as the reference. Predicted structures of CtiC homologues encoded by SGI1, IE*Vch*USA2, IME*Vch*USA3, and IE*Vch*USA5 are shown. (**D**) Structural similarity correspondence analysis of representative CtiC homologues and CTD of MOB_{H1} relaxases computed by the Dali server. The structural similarity matrix is shown in Fig. S5B. (**E**) to (**G**), 2-h mating assays between *E. coli* GG56 (Nx^r) containing pVCR94^{Sp} (donor) and *E. coli* CAG18439 (Tc^r) (recipient). Transconjugants were selected as Tc^r Sp^r (pVCR94), Tc^r Km^r (IME*Vch*USA3), or Tc^r Sp^r Km^r (Cotransfer) colonies. Crossbars show the mean and standard errors of the mean of three independent experiments. In E, donors harboured IME*Vch*USA3^{Km} (WT) or its Δ*ctiC3* mutant with (+) or without (-) pBAD30 expressing *ctiC3* (p*ctiC3*). In F, the donor expressed the designated *ctiC* from pBAD30. In G, the donor contained pVCR94^{Sp} (WT) or either its ΔMIBD (Δ) or ΔMIBD-*ctiC* (*ctiC*) *traI* mutants. Results for the 2-, 4- and 6-h mating assays are presented in Fig. S6. "x" indicates the frequency of transconjugant formation was below the detection limit

($<10^{-8}$). Statistical treatments are as described in Fig. 1D. Complete sets of P values are presented in Tables S4 to S6.

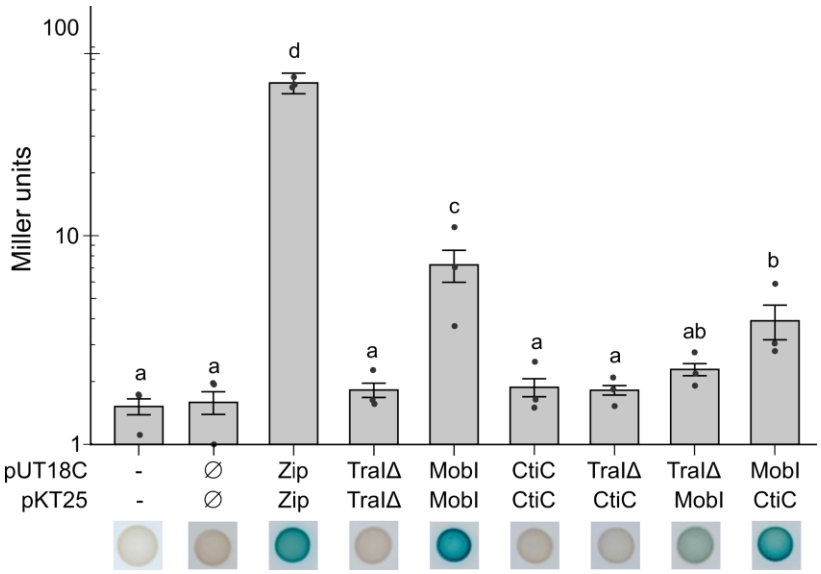

Figure 4. *In vivo* analysis of protein interactions using BACTH assays. MobI, TraI and CtiC interactions were quantified in *E. coli* BTH101 carrying plasmids encoding T18 and T25 C-terminal fusions. "-" and "∅" represent the negative controls BTH101 without plasmid and BTH101 carrying plasmids expressing T18 and T25 fragments not fused to a protein, respectively. Below the bars are shown the colonies grown on LB agar with IPTG and contained either pKT25-MobI and the designated pUT18C-TraIΔHD mutant or pKT25-zip and pUT18C-zip (positive control). The bars represent the mean β-galactosidase activities and standard error of the mean of three independent experiments. Statistical treatment is as described in Fig. 1D. The complete set of P values is presented in Table S7.

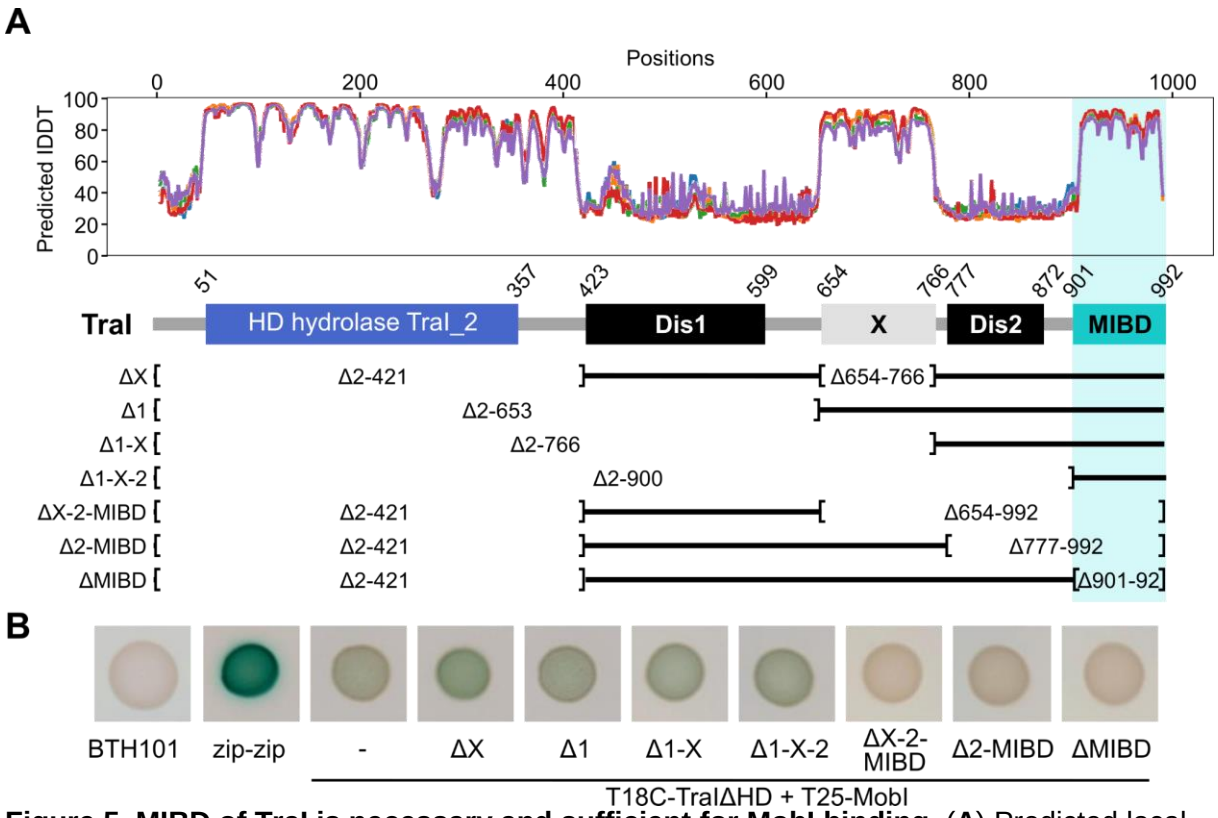

Figure 5. MIBD of TraI is necessary and sufficient for MobI binding. (**A**) Predicted local difference distance test (plDDT) plot of Alphafold2 structure predictions for pVCR94's TraI. Higher plDDT implies higher accuracy of the prediction. Matching domains and consensus disorder predictions (Pfam and MobiDB-lite) made by InterProScan are shown below the plDDT plot. X and MIBD were added manually based on Alphafold predictions. Brackets delimit the fragments removed in TraI for the BACTH assays. (**B**) β-galactosidase activities of BACTH assays. Colonies were grown on LB agar with IPTG and contained either pKT25-MobI and the designated pUT18C-TraIΔHD mutant or pKT25-zip and pUT18C-zip (positive control). Empty BTH101 was used as the negative control.

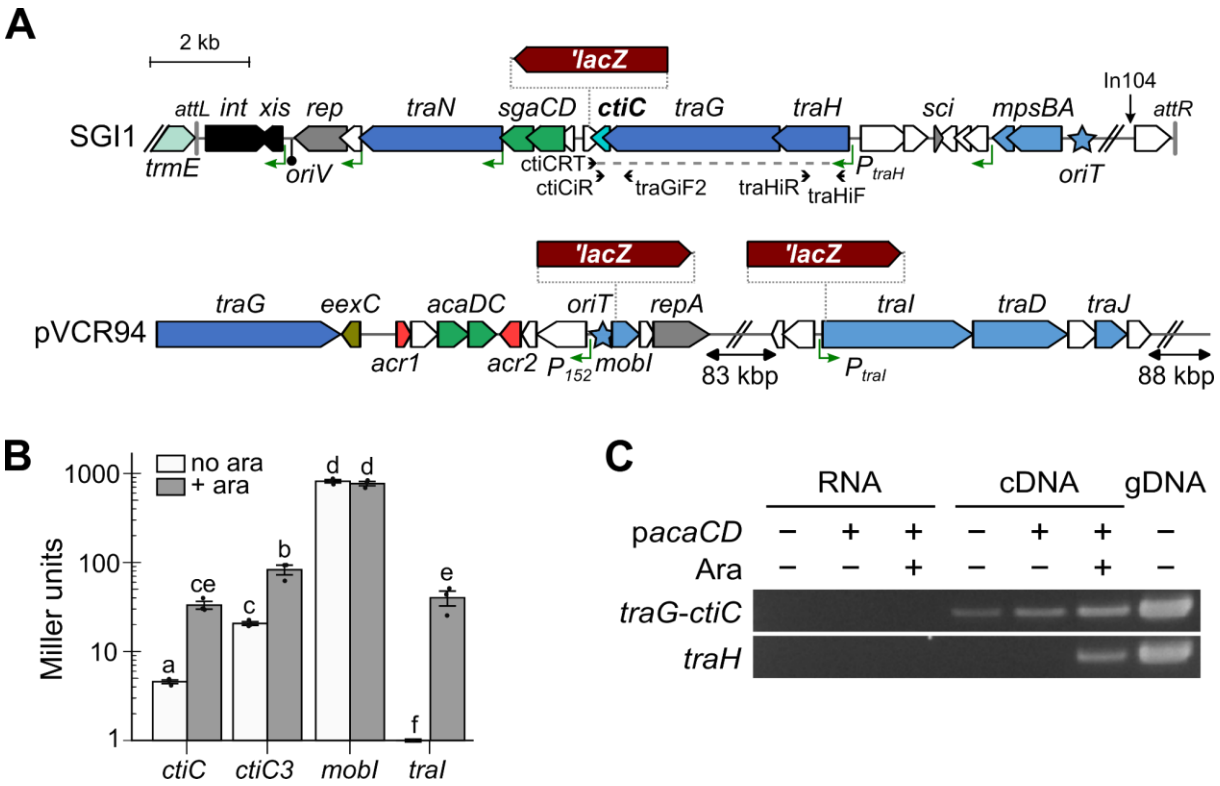

Figure 6. Comparative analysis of *ctiC*, *mobI*, and *traI* expression levels. (**A**) Schematic map of SGI1 and pVCR94 with the positions of the *lacZ* fusions. The *aad7* gene (Sp^r) downstream of *lacZ* is not shown. Genes are colour-coded as indicated in Fig. 1. AcaCD-responsive promoters are indicated by green angled arrows. The position and name of primers used for the reverse transcription assays are indicated by arrows. (**B**) β-galactosidase activities expressed in Miller units of the *ctiC*'-, *ctiC3*'-, *mobI*'-, and *traI*'-'*lacZ* translational fusions in response to AcaCD in arabinose-induced (grey) versus non-induced (white) strain bearing pBAD-acaDC. The bars represent the mean and standard error of the mean of three independent experiments. Statistical treatment is as described in Fig. 1D. The complete set of P values is presented in Table S8. (**C**) A 2% agarose gel of the PCR amplification of $traH_S$ and the junction between $traG_S$ and *ctiC* on the cDNA product. GG56 *trmE*::SGI1^{Km} genomic DNA (gDNA) and reverse transcription samples without reverse transcriptase (RNA) were used as positive and negative PCR controls, respectively.

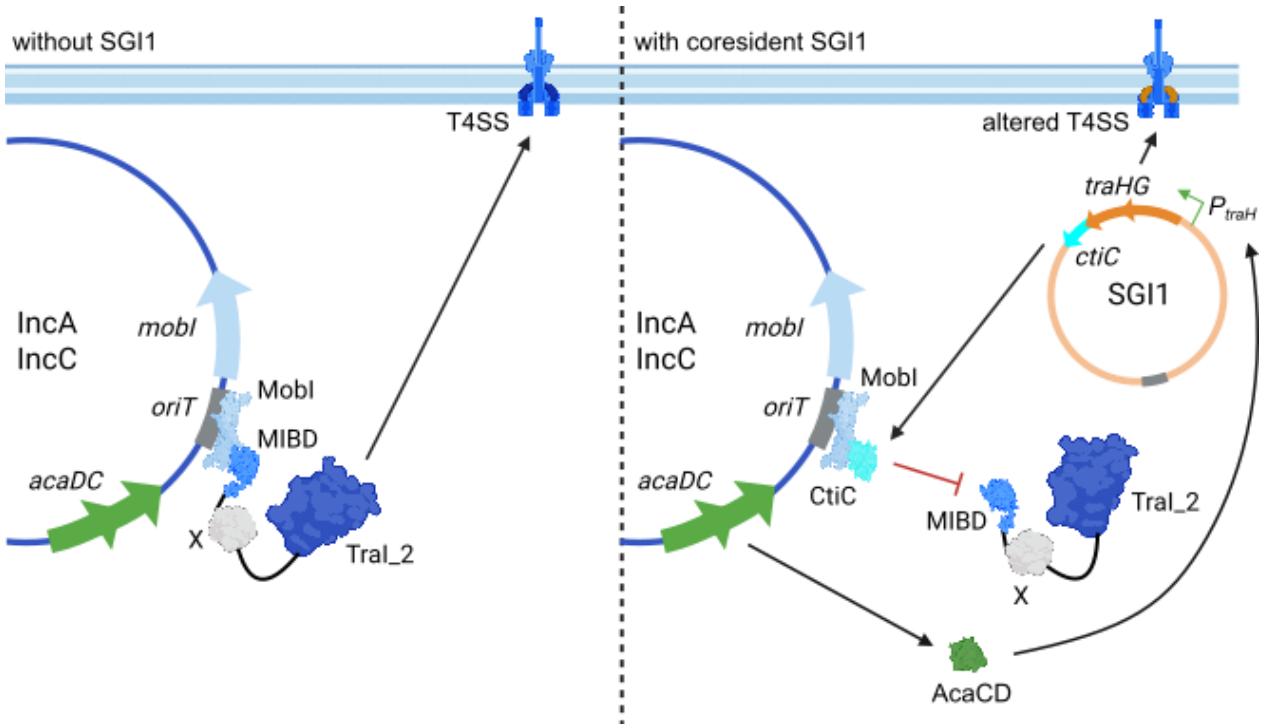

Figure 7. Model of fertility inhibition of IncA and IncC plasmids mediated by SGI1-like IMEs. CtiC competes with MIBD of TraI to bind to MobI, preventing the initiation of transfer at *oriT* of A/C plasmids when SGI1 is present. Since SGI1 encodes its own relaxase MpsAB, unrelated to the MOB_{H12} relaxase TraI, it is not subjected to inhibition by CtiC.

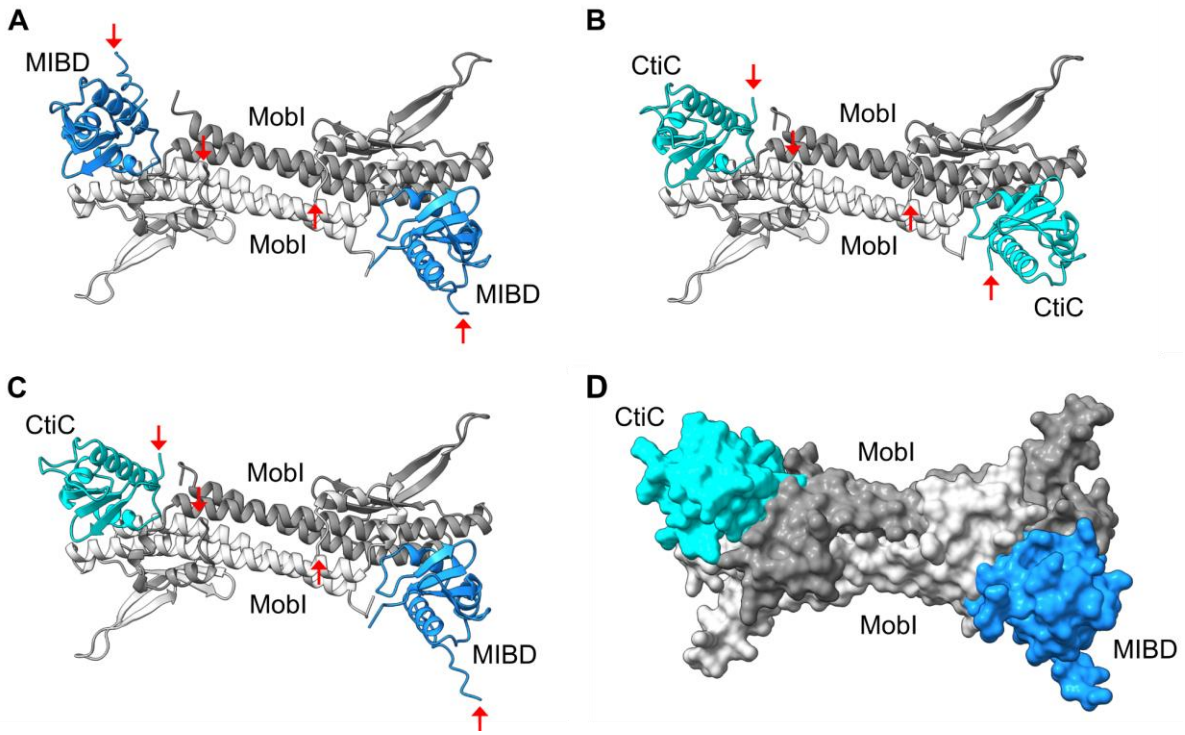

Figure 8. Predicted models of quaternary complexes formed between MobI, MIBD, and CtiC. Alphafold3 predictions of $MobI_2$-$MIBD_2$ (A), $MobI_2$-$CtiC_2$ (B), and MIBD-$MobI_2$-CtiC (C) complexes. The red arrows indicate the N-terminus of proteins. (D) Molecular surface prediction of the MIBD-$MobI_2$-CtiC complex.